Estrogen modulates mesenchymal-epidermal interactions in the adult nipple

Hsing-Jung Wu[1], Ji Won Oh[2,3,4], Dan F. Spandau[5], Sunil Tholpady[6], Jesus Diaz III[1], Laura J. Schroeder[1] Carlos D. Offutt[1], Adam B. Glick[7], Maksim V. Plikus [2], Sachiko Koyama[1] and John Foley[1,4]

1. Medical Sciences Program, Indiana University School of Medicine, Bloomington, IN, USA

2. Department of Developmental and Cell Biology, Sue and Bill Gross Stem Cell Research Center, Center for Complex Biological Systems, University of California Irvine, Irvine, CA, USA

3. Department of Anatomy, School of Medicine, Kyungpook National University, Daegu, Korea

4. Biomedical Research Institute, Kyungpook National University Hospital, Daegu, Korea

5. Department of Dermatology, Indiana University School of Medicine, Indianapolis, IN, USA

6. Department of Surgery, Indiana University School of Medicine, Indianapolis, IN, USA

7. Department of Veterinary and Biomedical Sciences, The Pennsylvania State University, University Park, PA 16802, USA

Corresponding Author: John Foley
Medical Sciences
Indiana University
Jordan Hall
Bloomington, IN 47405
Phone: 812-855-3189
E-mail: jgfoley@indiana.edu

Key words:

Fibroblast, nipple, estrogen receptor-alpha, TGFβ, epidermis

Summary statement

Distinct epidermis of specialized skin regions, such as the nipple is patterned and maintained by signals from the underlying fibroblasts. Here we establish the inductive potential and transcriptional prolife of adult nipple fibroblasts.

Abstract

Maintenance of specialized epidermis requires signals from the underlying mesenchyme; however, specific pathways involved remain to be identified. By recombining cells from ventral skin of the *K14-PTHrP* transgenic mice with those from wild-type, we show that transgenic stroma is sufficient to reprogram wild-type keratinocytes into nipple-like epidermis. To identify candidate nipple-specific signaling factors, we compared gene expression signatures of sorted Pdgfrα-positive ventral *K14-PTHrP* and wild-type fibroblasts, identifying differentially-expressed transcripts of the WNT, HGF, TGFβ, IGF, BMP, FGF and estrogen signaling. Considering that some of the growth factor pathways are targets for estrogen regulation, we examined the hormone's upstream role in maintaining the nipple. Ablation of estrogen signaling by ovariectomy produced nipples with abnormally thin epidermis, and we identified TGFβ as a negatively regulated target of estrogen signaling. Estrogen treatment represses Tgfβ1 at the transcript and protein levels in *K14-PTHrP* fibroblasts *in vitro,* while ovariectomy increased *Tgfβ1* in *K14-PTHrP* ventral skin. Moreover, ectopic delivery of Tgfβ1 protein into nipple connective tissue reduced epidermal proliferation. Taken together, specialized nipple epidermis is maintained by estrogen-induced repression of TGFβ signaling in the local fibroblasts.

Introduction

Vertebrates interact and manipulate their environment using regions of specialized skin. Epidermis in such specialized skin sites often has distinct stratification patterns, expresses unique differentiation markers, and features novel appendages (Billingham and Silvers, 1967). In humans, such sites include nipples, lips, palms, soles, anal and genital skin (Schweizer et al., 1984). Mice share these sites and also feature distinct tail, muzzle and ear skin (Schweizer, 1993). Among these, the nipple stands out for its pivotal role in the mammalian life cycle as a key site for milk removal from mother to offspring. Thickened and highly proliferative, nipple epidermis is uniquely adapted to withstand high mechanical and frictional forces associated with milk delivery (Eastwood et al., 2007; Koyama et al., 2013; Mahler et al., 2004), and it expresses a unique set of keratins and intermediate filament associated proteins, largely absent in the trunk epidermis (Eastwood et al., 2007; Mahler et al., 2004). Despite its important function and unique characteristics, little is known about how this epidermal differentiation state is acquired and maintained.

Generally, epithelial specialization is thought to require inductive signals from the underlying connective tissue (Dhouailly et al., 1998). For example, seminal experiments conducted by the Billingham group found that grafts of sole dermis recombined with ear or trunk epidermis produced a thickened and expanded cornified layer, indicating that the mesenchyme specifies the phenotype of the grafted epithelium (Billingham and Silvers, 1967). In other classic experiments, recombination of the palatal epithelium with the cheek connective tissue or *vice versa* resulted in the *de novo* keratin expression pattern normally associated with the connective tissue type (Mackenzie and Hill, 1981, 1984; Schweizer et al., 1984).

Additionally, grafting of the non-palmoplantar epidermal cells onto human injured soles led to epidermis adopting palmoplantar phenotype, complete with the expression of the site specific keratin K9 (Yamaguchi, 1999). The lead role of fibroblasts in determining palmoplantar characteristics of the associated epidermis was further confirmed in follow-up experiments (Yamaguchi, 1999). These classic studies suggest a central role for fibroblasts in determinng the anatomical specificity of epidermal cell fate and characteristics.

The inductive and maintenance growth factors produced by site-specific and appendage-specific skin fibroblasts are just starting to be defined (Driskell et al., 2013; Driskell and Watt, 2015; Sriram et al., 2015). Perhaps, the most well-studied in this respect are the dermal papilla fibroblasts of the hair follicle, that induce both the formation (Jahoda et al., 1984; Jahoda et al., 1993; Plikus, 2014; Yang and Cotsarelis, 2010) and regenerative cycling of hair follicles (Chi et al., 2013; Clavel et al., 2012; Enshell-Seijffers et al., 2010; Morgan, 2014; Rendl et al., 2005; Sennett and Rendl, 2012). Dermal papilla fibroblast-specific factors are fibroblast growth factors Fgf7 and Fgf10 (Chi et al., 2013; Clavel et al., 2012; Enshell-Seijffers et al., 2010; Morgan, 2014; Rendl et al., 2005; Sennett and Rendl, 2012), bone morphogenetic proteins Bmp4 and Bmp6 (Clavel et al., 2012; Rendl et al., 2005; Rendl et al., 2008), BMP antagonists noggin (Botchkarev et al., 1999; Botchkarev et al., 2002; Rendl et al., 2005), transforming growth factor TGFβ2 (Oshimori and Fuchs, 2012), and many others (Morgan, 2014; Rendl et al., 2005; Sennett and Rendl, 2012). Outside of the hair follicle, skin fibroblasts also feature significant specialization and heterogeneity; however, our understanding of their molecular profiles is still rudimental (Driskell et al., 2013; Driskell and Watt, 2015; Sriram et al., 2015). For instance, recent studies show that papillary (upper) dermis fibroblasts

express higher levels of growth factors that control epidermal proliferation and differentiation, whereas those from the reticular (lower) dermis produce high levels of signaling molecules associated with matrix production (Driskell et al., 2013; Driskell and Watt, 2015; Sriram et al., 2015). These findings imply that transcriptional heterogeneity may be an intrinsic property related to the developmental history of specific fibroblasts. The notion is further supported by the transcriptional profiling studies on skin fibroblasts from different anatomical locations (Chang et al., 2002; Rinn et al., 2006; Rinn et al., 2008). Signature profiles of regionally specific skin fibroblasts are in part maintained by their unique homeobox (HOX) gene activities. For example, in human skin the HOXB genes are expressed in the trunk and non-dermal fibroblasts, whereas HOXD4 and HOXD8 are found exclusively in trunk and proximal leg fibroblasts. Intriguingly, HOXA13 is limited in expression to fibroblasts in distal body sites including hands, feet and foreskin, and its activity is required for the expression of the distal-specific Wingless-Int family growth factor WNT5A (Chang et al., 2002; Rinn et al., 2006; Rinn et al., 2008). In mice, differential expression of the HOX gene Tbx15 between dorsal and ventral skin fibroblasts contributes to the differential skin pigmentation along the sagittal body axis (Candille et al., 2004). Taken together, these findings imply that the developmental history of fibroblasts profoundly impacts their inductive and maintenance interactions with the epidermis.

The specific developmental origin of the nipple connective fibroblasts that underlie the structure has not been completely established. The mammary gland develops at the interface of what will become dorsal and ventral skin. The mesenchymal cells that underlie the mammary line at E10.5, may be derived from the hypaxial mesoderm (Dhouailly and Oftedal, 2016; Oftedal and Dhouailly, 2013). However, it is not clear whether these or other cells condense around the bud as the

primary mammary mesenchyme at E11 to E12.5 (Sakakura, 1987; Sakakura et al., 1987). The differentiation of the mammary mesenchyme is driven in part by PTHrP signaling from the developing epithelial cells via PTH/PTHrP receptor expessed on the stroma. In turn, inductive signaling from these differentiated fibroblasts is required to produce nipple sheath, which is of distinct evolutionary origin from the gland (Oftedal and Dhouailly, 2013) at E17 (Dunbar et al., 1999; Dunbar and Wysolmerski, 1999; Wysolmerski et al., 1998). Intriguingly, ectopic expression of PTHrP driven by the human Keratin 14 promotor in *K14-PTHrP* mice (*aka* KrP mice) dramatically expands the differentiation of the lateral plate mesoderm derivatives to the mammary mesenchyme fate. However, this has minimal impact on cells of the dorsal dermis (Foley et al., 2001). In part, this appears to be the result of increased Bmp4 signaling in the developing ventral skin of the embryo, driving mammary mesenchyme differentiation (Hens et al., 2007). However, other factors such as timing of trangene expression or sensitivity of somitic versus lateral plate-derived mesenchymal cells to PTHrP may be involved (Foley et al., 2001). In the adult female mouse, the ectopic expression of PTHrP results in a hairless skin with a thickened epidermis and complex connective tissue consistent with the nipple (Abdalkhani et al., 2002; Foley et al., 2001; Foley et al., 1998). Whether the fibroblasts that underlie the nipple are simply derived from mammary mesenchyme cells remains to be determined. Nevertheless during skin development these cells appear to have the capacity to induce and maintain the specialized epidermis that characterizes the structure (Foley et al., 2001; Wu et al., 2015).

In this study, we set out to define the inductive and signaling properties of the specialized fibroblasts from the nipple skin. We established that KrP fibroblasts robustly induce reprograming of the trunk epidermis toward nipple fate. We also

established the unique transcriptional signature of the KrP fibroblasts and evaluated the impact of key pathways identified by that analysis.

Results

Fibroblast-induced reprogramming of trunk keratinocytes into nipple-like epidermis

The instructive capacity of highly specialized nipple fibroblasts, however, has not been established and this has been limited by the very small size of the appendage in mice. To determine if nipple fibroblasts have the capacity to reprogram the fate of trunk epidermis, a grafting experiment was carried out using purified cells from ventral skin of neonatal female KrP mice (Wysolmerski et al., 1994), in which close to 1/4 of the entire body's skin is nipple-like (Foley et al., 2001). KrP fibroblasts were recombined with wild-type (WT) neonatal trunk keratinocytes from both dorsal and ventral skin. The resulting grafts were compared to those reconstituted from WT epidermal and dermal cells, as well as the ventral skin of KrP mice (Fig. 1A) (Lichti et al., 2008). When WT keratinocytes and WT fibroblasts were grafted, hairy skin was produced, as previously reported (n=3) (Fig. 1B, left) (Lee et al., 2011; Lichti et al., 2008; Lichti et al., 1995; Lichti et al., 1993). As expected, reconstitution of KrP neonatal keratinocytes with KrP fibroblasts produced pigmented nipple-like skin with a thickened epidermis and without hair follicles (n=3) (Fig. 1B, 1C, right panels). Importantly, grafts that recombined WT neonatal keratinocytes with KrP fibroblasts also resulted in pigmented nipple-like skin (n=3) with similar histology to those reconstituted from KrP cells only (Fig. 1B, third panel and 1C, middle panel). As shown on Fig. 1D and 1E, grafts that contained KrP ventral fibroblasts expressed

nipple epidermis-specific markers, keratin K2e, and expanded filaggrin, whereas WT cell only grafts did not. In normal haired mouse skin melanocytes localize exclusively to hair follicles (Quevedo and Fleischmann, 1980). In contrast, connective tissue of grafts based upon ventral KrP dermal cells contained pigmented cells that we have previously determined to be melanocytes (Abdalkhani et al., 2002) (Fig. 1C, arrows). Thus, dermal cells from KrP ventral skin produce a signaling environment sufficient to induce reprogramming of neonatal trunk keratinocytes toward nipple-like epidermis, and formation of pigmented connective tissue.

Pdgfrα is a marker for nipple fibroblasts

Platelet-derived growth factor receptor α (Pdgfrα) was previously reported to be a useful marker for isolating dermal fibroblasts from haired skin (Collins et al., 2011). Here, using immunofluorescence, we show that Pdgfrα is expressed in nipple fibroblasts, but not in basal keratinocytes or fibroblasts in WT ventral skin. It is also expressed in ventral dermis of KrP mice (Fig. 2A). Next we evaluated Pdgfrα staining along with staining for fibroblast marker vimentin and found substantial overlap (Fig. 2B). Dual staining for smooth muscle marker Acta2 and Pdgfrα revealed co-expression in blood vessels, arrector pili muscles, smooth muscle-like cells along the lactiferous duct of the nipple, and nests of contractile cells within KrP ventral dermis. This data indicates that Pdgfrα can be used as a marker for isolating specialized fibroblasts from KrP ventral skin, however the Pdgfrα-positive fraction will also include some, albeit few Acta2-positive vascular and muscle cells.

Next, fibroblasts were isolated on cell sorting (FACS) from the nipple-like skin of virgin adult female KrP mice and ventral skin of their WT littermates, respectively using anti-Pdgfrα (*aka* anti-CD140) antibody (Fig. 3A). To purify $CD140^{hi}$ population,

we set up a dump channel to exclude cells expressing CD31 (endothelial cells), CD117 (melanocytes), CD45 (hematopoietic cells) or CD49f markers (keratinocytes) (Collins et al., 2011). Next, we harvested both WT and KrP RNAs from three distinct cell populations: $CD140^{hi}$/$dump^{-}$ cells, $CD140^{-}$/$dump^{+}$ cells and viable cells expressing none of the markers (Fig. 3B). There was also almost a two-fold increase of *Pdgfrα* and an elevated expression of *Vim* and *Col1a2* in KrP comparing to WT $CD140^{+}$ sorted cells. Next, sorted $CD140^{+}$ or $dump^{+}$ cell populations were transiently cultured for 48 hours. While cultured $CD140^{+}$ cells had branched cytoplasm and elongated, spindle-like shape, morphologically similar to a typical fibroblast, $dump^{+}$ cells, were mostly epithelial in appearance (Fig. 3C *vs.* 3D). (Kalluri and Zeisberg, 2006). Thus, we confirmed that Pdgfrα is expressed highly on dermal fibroblasts from the ventral skin of both WT and KrP female mice and that it can be used as a marker for their isolation by sorting.

Microarray profiling reveals a unique gene expression signature of KrP fibroblasts

To identify candidate inductive and maintenance factors present in nipple fibroblasts, we performed microarray-based transcriptome profiling on FACS-sorted $CD140^{+}$ fibroblasts from KrP and WT ventral skin. 123 genes were upregulated and 118 were downregulated in KrP as compared to ventral WT fibroblasts. To identify signaling pathways altered in KrP fibroblasts, differentially expressed genes were subjected to Gene Ontology (GO) analysis and altered signaling of WNT, HGF, TGFβ, IGF, BMP and FGF pathway elements were identified (Fig. 4 Fig. S1). Interestingly, selected extracellular matrix transcripts, including *Col1a*, as well as metalloproteinase inhibitors *Timps* were upregulated, while several metalloproteinase genes were downregulated in the KrP fibroblasts.

The differential expression of 30 transcripts (20 increased, 6 decreased and 4 unchanged in KrP relative to WT fibroblasts), many of which are part of the pathways identified by the Ingenuity and GO term analysis, was largely confirmed by qRT-PCR using sorted fibroblasts as well as micro-dissected virgin WT nipples, WT and intact KrP ventral skin. (Fig. S2 and S3). We grew both WT and KrP ventral fibroblasts *in vitro* for up to 5 passages. and found signature genes remained differentially regulated in KrP relative to WT ventral fibroblasts (Fig. S4). Overall, differential expression of most genes that comprise the KrP fibroblast signature are consistent in the nipple and stable in primary culture (Rinn et al., 2006; Rinn et al., 2008).

Estrogen receptor signaling in fibroblasts maintains nipple structure

Fibroblasts associated with the mammary gland in mice have long been recognized to be responsive to estrogen (Hiremath et al., 2012) (Cunha et al., 1997). (Wu et al., 2015). Not surprisingly, pregnancy and lactation related hormone receptors, including progesterone receptor *(Pgr)*, oxytocin receptor *(Oxtr)*, and relaxin receptor *(Rxsp1)* were strongly upregulated in the nipple-like KrP fibroblasts on the microarray analysis (Fig. 5A). Since both oxytocin and progesterone receptors are regulated by estrogen (Lapidus et al., 1998; Zingg et al., 1998), we next performed qRT-PCR analysis on these hormone receptor-regulated genes using intact ventral skin, as well as sorted fibroblasts. Indeed, transcripts for *Esr1*, *Oxtr* and *Pgr* were significantly increased in the WT nipple and KrP nipple-like ventral skin relative to WT non-nipple skin (Fig. 5B). Similar results were also observed for the $CD140^{+}$ sorted KrP fibroblasts (Fig. 5B). Focusing on Esr1, its differential expression between primary cultured fibroblasts from WT *vs.* KrP virgin female ventral skin was confirmed at the protein level on the Western blot (Fig. 5C) and in the intact WT

nipple and by immunofluorescence (Fig. 5D). At the cellular level, nipple fibroblast had robust nuclear Esr1 expression (Fig. 5D) (McCormack and Greenwald, 1974). These findings suggest that nipple fibroblasts, including these from the KrP mouse model, maintain stable Esr1 expression and are the target sites for estrogen action.

To further investigate the role of ovarian hormones in the nipple, we ovariectomized (ovex) pre-pubertal WT and KrP mice and then harvested nipples and KrP ventral skin between 1.5 to 3 months later. We now show that the nipple epidermis in ovexed mice is much thinner than in controls, and the basal layer is less markedly invaginated (Fig. 5E). These changes were accompanied by the diminished expression of the nipple epidermal markers, K2e and filaggrin (Fig. 5F Fig S5). Moreover, nipple size, largely controlled by extracellular matrix (Wu et al., 2015), was ~30% smaller in the ovexed WT mice as compared to age-matched controls, and specialized nipple connective tissue, typically composed of small tightly packed collagen bundles, was markedly diminished in the ovexed KrP mice (Fig. 5E). Thus, the removal of ovarian hormones, including estrogens, impacts both the epidermis and the connective tissue of the nipple.

TGFβ signaling is downregulated in KrP fibroblasts

In reviewing the growth factor pathways differentially represented in the KrP fibroblasts by GO analysis, we found that several of them can be regulated by estrogen in non-nipple tissues (Hewitt et al., 2010; Knabbe et al., 1987; Yokota et al., 2008). Among these is the TGFβ pathway, which has been shown to be inhibited by estrogen signaling components at multiple levels (Cherlet and Murphy, 2007; Colletta et al., 1990), including repression of ligand secretion (Knabbe et al., 1987). This prompted us to evaluate Tgfb1 production and signaling in the context of nipple

tissue further. Indeed, *Tgfb1* transcript was decreased by 50% in sorted KrP fibroblasts as compared to WT ventral skin fibroblasts (Fig. 6A). Similar decrease, by ~70%, was found in intact WT nipple and KrP skin as compared to ventral WT skin of virgin mice (Fig. 6A). To further validate reduced TGFβ signaling, we examined the expression levels of TGFβ-specific phospho-Smad2/3 (pSmad2/3). We show that while nuclear pSmad2/3 expression was observed in most of the ventral skin fibroblasts, but less nipple fibroblasts were positive (Fig. 6B). Secreted Tgfb1 protein (as measured by ELISA) was reduced by ~50% at 48 or 72 hours of culture of primary KrP *vs.* WT ventral skin fibroblasts (Fig. 6C), while *Tgfb1* transcript expression remained stably reduced in cultured primary KrP fibroblasts (Fig. 6C) and this was maintained for 4 passages (not shown). On Western blot, pSmad2/3, but not total Smad2/3 protein was reduced in KrP *vs.* WT cultured fibroblasts (Fig. 6D). Taken together, these data suggest TGFβ signaling is downregulated in nipple fibroblast.

Estrogen regulates Tgfb1 transcript levels in KrP fibroblasts

To further establish a functional relationship between estrogen and TGFβ signaling in nipple fibroblast, we employed primary fibroblast culture in stripped serum phenol-red free media. WT or KrP fibroblasts were treated with 0.5 or 10 nM estradiol for 48 or 72 hours, followed by qRT-PCR analysis. For KrP fibroblasts culture, removal of phenol-red, a known weak estrogen mimetic, resulted in *Tgfb1* transcript to increase by 50%, whereas addition of 0.5 nM estradiol lowered *Tgfb1* to baseline level and 10nM estradiol reduced it by another 50% (Fig. 6E). We also validated estradiol's effect on Tgfb1 at the protein level by ELISA measurements. While the serum free conditions reduced total Tgfb1 levels in both WT and KrP

fibroblasts, addition of 10 nM of estradiol decreased the protein by 40% in cultures of KrP fibroblasts only (Fig. 6F). Taken together, these *in vitro* assays demonstrate that *Tgfb1* production is specifically repressed by exogenous estradiol in the KrP fibroblast.

Next, we evaluated TGFβ signaling in an *in vivo* system with altered estrogen signaling, the ovexed KrP mice. As shown in Fig. 6G, *Tgfb1* transcript was elevated four-fold in the ventral skin of KrP mice that had been ovexed for 16 weeks, whereas the estrogen regulated *Esr1* and *Pr* were reduced by 50% as compared to age matched samples from intact female KrP mice. On Western blot, pSmad2/3 protein was elevated in ovexed *vs.* non-ovexed KrP mice (Fig. 6H, S6), indicating signaling downstream of TGFβ was elevated in KrP skin under conditions of low estrogen.

Dermal but not epidermal Tgfβ partially shifts nipple features towards trunk skin

To initially test the impact of Tgfβ on nipple skin, slow peptide-releasing beads were implanted into 8-week old virgin female mouse skin. Beads with or without 0.2 µg of murine recombinant Tgfb1 were implanted into the nipple dermis of WT mice or ventral skin of KrP mice and their effect was analyzed after 7 days. In contrast to buffer-treated control beads, Tgfb1-treated beads showed a trend toward a thinner epidermis in WT nipple and KrP skin and a thinner papillary dermal layer in the transgenic (Fig. 7C). This was accompanied by significant decrease in epidermal BrdU labeling by ~50%. In this experiment, Tgfb1 did not have measurable impact on WT non-nipple skin (Fig. 7C). To investigate whether Tgfb1 overexpression could directly influence nipple epidermis, we used doxycycline to induce transgene expression in the *K14-rTA/tetO-TGFb1* mice (Liu et al., 2001), which produces a non-latent porcine form of the ligand. As shown in Fig. S7 and S8, nipple epidermal

thickness and BrdU incorporation were similar in transgene expressing and non-induced double transgenic mice, whereas BrdU incorporation was substantially reduced in the ventral skin of TGFb1 overexpressing mice. Taken together, it appears that overexpression of TGFb1 within the dermis rather than the epidermis has a greater impact on nipple skin.

Discussion

In this work we have defined key molecular and cellular attributes of the fibroblast population that underlie specialized epidermis of the murine nipple. First, we showed that fibroblasts from newborn KrP mice induce reprogramming of WT trunk skin keratinocytes toward nipple fate. Secondly, we identified unique gene expression signature of the KrP fibroblasts. Next, we showed that Esr1 signaling is among the major pathways active in KrP fibroblasts and that it signals to suppress TGFβ signaling in KrP fibroblast *in vitro*. We also present the evidence suggesting that reduced TGFβ pathway activity is essential for endowing nipple skin with its unique characteristics in the adult.

To-date, palmoplantar fibroblasts are the most well-defined example of site-specific skin fibroblasts. Their ability to induce reprogramming of keratinocytes into thickened epidermis with unique keratin expression pattern (Yamaguchi, 1999), was attributed to several secreted factors. One of them is Dkk1, a soluble inhibitor of canonical WNT signaling (Yamaguchi et al., 2004; Yamaguchi et al., 2009; Yamaguchi et al., 2008), which also functions to reduce pigmentation of palms and soles by inhibiting melanocyte activity (Yamaguchi et al., 2004; Yamaguchi et al.,

2009). Another factor is the non-canonical WNT ligand Wnt5a, a putative downstream target of Hoxa13 (Rinn et al., 2006; Rinn et al., 2008). Here, we provide the first insight into the signaling network that defines site-specific properties of nipple fibroblasts.

Our recombination experiments confirm the leading role of fibroblasts in endowing skin with its regional specificity. We show that KrP stromal cells reprogram WT trunk skin keratinocytes to have nipple-like features, including stratification pattern and marker profile. It is noteworthy that our KrP stromal cells grafts were pigmented, similar to WT nipple and intact KrP ventral skin (Abdalkhani et al., 2002). This suggests that fibroblasts regulate site-specific skin pigmentation pattern, consistent with the previous experiments on palmoplantar fibroblasts (Yamaguchi et al., 2004; Yamaguchi et al., 2009).

Commonly, specialized skin sites in mammals undergo physiological changes in adult life. For instance, palmoplantar skin responds to weight bearing by altering epidermal proliferation dynamics to produce a thick, protective callus (Menz et al., 2007). Perineal skin in the anogenital region of the Old World monkeys can dramatically change in synchrony with the altered reproductive states (VandeBerg et al., 2009). The human nipple and areola skin increases in size and pigmentation during pregnancy and lactation (Javed and Lteif, 2013; Neifert et al., 1990). Estrogen is at moderate levels during nipple morphogenesis and Esr1 is dispensable for its formation (Bocchinfuso and Korach, 1997). Our new data from the ovexed mice indicate that estrogen signaling in fibroblasts is necessary for maintaining the thickened epidermis and some connective tissue features of the adult virgin nipple

(Fig. 5). Nipple expands during late pregnancy, when estrogen levels peak, and this is accompanied by high levels of nuclear Esr1 in the fibroblasts (Wu et al., 2015). This prompted us to speculate that estrogen likely triggers changes in the signaling environment required for the production of adult nipple connective tissue, its expansion and maintenance of the unique thickened epidermis. Among several candidate pathways identified in our transcriptomic studies, we focused on the reduction of the TGFβ signaling because it has known effects on fibroblast biology, including regulation of extracellular matrix production, modulation of growth factor secretion, including keratinocyte growth factor and colony stimulating factor Csf1, which are crucial for the regulation of epidermal proliferation and differentiation (Mauviel, 2009; Szabowski et al., 2000). Consistent with this, we now show that short term Tgfb1 bead implantation into the WT nipple and KrP ventral dermis reduced epidermal proliferation, whereas epidermal overexpression of the growth factor failed to do so. One caveat to these Tgfb1 studies is that they both produced a simple ligand in contrast the more complex endogenous form, involving the latency associated peptide as well as latent TGFβ-binding proteins (Robertson et al., 2015). Nevertheless, these findings imply that at least some aspects of the adult nipple epidermal phenotype can be reversed by ectopic activation of the TGFβ signaling and this appears to be an indirect effect of reduced autocrine TGFβ activity in nipple fibroblasts (Mauviel, 2009). We posit that further studies on some of the signaling pathways revealed here could lead to novel regenerative and tissue engineering approaches to nipple replacement.

Material and Methods

Mice

The *K14-PTHrP* (KrP) transgenic line (Wysolmerski et al., 1994) was maintained by continual breeding against unrelated C57BL/6 mice. WT mice used in this study were either inbred C57BL/6 or littermates of the KrP mice. All animal use was approved by the Indiana University Institutional Animal Care and Use Committee and was performed in compliance with stipulations of that body. *K14-rTA/tetO-TGFb1* mice were fed 1 g/kg doxycycline chow (Bio-Serve, Flemington NJ) for 3 weeks to induce transgene expression. Nipples and skin were harvested after BrdU injection (see below). Inbred 1.5 to 3 month old *Foxn1*$^{nu/nu}$ BALB/c mice (NU/J Jackson Labs, Bar Harbor, ME) were used as recipients of grafts.

Grafting

One- to two-day-old pups derived from the mating of KrP male and WT female mice were used to isolate keratinocytes and fibroblasts following the protocols developed by Lichti, Yuspa and colleagues (Lichti et al., 2008; Lichti et al., 1995; Lichti et al., 1993; Weinberg et al., 1993). After genotyping, the ventral skin was exclusively used from KrP positive female pups whereas the entire trunk skin was used from WT pups. The grafts were composed of 1X10^{7} fibroblasts and 1-2X10^{6} keratinocytes. These were mixed together and applied onto Integra® Dermal Regeneration Template (Integra, Plainsboro NJ) and incubated 1 to 2 hours prior to placing on the mouse. The grafting procedure followed the method of (Lee et al., 2011). Grafts were harvested 2 to 4 months after the surgery. For each round of grafts, WT epidermal and dermal cells were grafted alone to ensure that hair shafts were not produced, which indicated purity of the cellular preparations (not shown).

Isolation of adult fibroblasts

Primary fibroblasts were isolated as previously described (Lichti et al., 2008; Wu et al., 2015). Briefly, ventral skin with mammary glands was carefully dissected of 6-8 week-old female virgin WT or KrP mice and was floated on 0.25% trypsin (Gibco Thermo Fisher Scientific, Waltham, MA) overnight at 4°C. The next day, epidermis was removed, the remaining tissue was minced, and enzymatically digested in a collagenase mixture. The retained cells were then centrifuged at 150 g for 5 min, and the supernatant was further pelleted at 450 g for 5 min. Next, pellets from both 150 g and 450 g spin-down were pooled together and washed with DMEM twice, then centrifuged at 230 g for 5 min before being strained through a 45 μm mesh. The retained cells were suspended in DMEM and plated at $1x10^6$ per 100 mm dish. Additional information on media and chemicals used can be found in the supplemental methods.

Flow Cytometry

The isolated cells were labeled with anti-mouse CD140a-APC (17-1401-81, eBioscience San Diego, CA), anti-mouse CD31-(PECAM-1)-PE (12-0311, eBioscience, San Diego, CA), anti-mouse CD45-PE (12-045, eBioscience, San Diego, CA), anti-mouse CD117-(c-kit) -PE (12-1171, eBioscience, San Diego, CA) and anti-human/anti-mouse CD49f-(Integrin alpha6)-PE (12-0495, eBioscience, San Diego, CA) (Collins et al., 2011)(antibodies according to manufacturer's instruction. Meanwhile, 7-aminoactinomycin D (7-AAD) viability staining was performed to exclude dead cells. Cells without antibody labeling and cells with only secondary antibody labeling were used as controls to set the gates. $CD140^+$ cells were collected using flow cytometry sorter with FACSDiva software, FACSAria II (BD

Biosciences, San Jose, CA) sorter. FACS analysis was evaluated by FlowJo version X (FlowJo LLC, Ashland, OR). Re-analysis of the sorted cells indicated a 96-98% purity of $CD140^+$ cells.

Gene expression profiling/micro-array

Total RNA from $CD140^+/dump^-$ dermal fibroblasts from WT or KrP ventral skin of three independent groups, each using 5 WT and 3 K14-PTHrP female mice were purified as described above. RNA quality was measured by 2100 Bioanalyzer (Agilent Technologies, Santa Clara, CA), and RNA quantity was accessed by Qubit® 2.0 Fluorometer (Q32866, Thermo Fisher Scientific, Waltham, MA). 20 ng of RNA with RNA integrity number (RIN) ≥ 8 were subjected to reverse transcription and hybridization to Affymetrix Mouse Gene 2.0 ST Arrays. Gene expression data was processed and analyzed using Affymetrix Microarray Analysis Suite Version 5.0 (MAS5.0). Data is available at GEO: GSE87030 (URL: https://www.ncbi.nlm.nih.gov/geo/query/acc.cgi?acc=GSE87030). To identify differentially expressed genes, gene expression was compared between WT and KrP group in each experiment using a cut-off value of p-value less than 0.05 in two tail t-test and fold change over 2 fold. Principal component analysis and Volcano plot were conducted by R software package. Differentially expressed genes were then subjected for hierarchical clustering as well as pathway prediction analysis using Network2Canvas, respectively (Tan et al., 2013).

ELISA for Tgfb1

$5x10^5$ WT or KrP primary fibroblasts were seeded in 10 cm dishes in DMEM growth media (Sigma-Aldrich, St Louis, MO) supplemented with 10% FCS, 100 U/ml penicillin and 100 ug/ml streptomycin overnight for attachment and then serum starved 12 hours. Supernatants were collected 48 and 72 hours after incubation and centrifuged at 13,000 rpm for 10 min at 4°C to remove any debris and stored at -80°C until used. Samples were measured using mouse Tgfb1 Quantikine ELISA (MB-100B, R&D Systems, Inc., Minneapolis, MN) following the manufacturer's instruction. Cells were counted after supernatants were harvested, and levels of Tgfb1 measurements were normalized to the cell number. Each experiment was carried out in triplicate.

Tgfb1 *agarose bead preparation/ implantation*

Recombinant mouse Tgfb1 (7666-MB-005, R&D systems, Minneapolis, MN) was lyophilized with 0.1% bovine serum albumin (BSA) and stored at -20°C until use. 4 mM of HCl was used to reconstitute recombinant Tgfb1 to a final concentration of 5-10 µg/mL. 250 µL of Affi-Gel Blue beads (100-200 mesh, Bio-Rad, Hercules, CA) were soaked in 250 µL of 10 µg/mL Tgfb1 and incubated at 37°C for one hour. Beads soaked with lyophilized BSA reconstituted in 4mM HCl were used as controls. 150 µl agarose bead suspensions were then injected into the ventral skin of WT and KrP mice, ages 8 weeks old, using 22-gauge needle. Sites of agarose bead implantation and the surrounding area of the implantation was harvested after 7 days.

Histology and immunofluorescence

Samples were collected, fixed and sectioned as previously described (Wu et al., 2015). Fluorescent microscope images were obtained with a Nikon NiE (Nikon Instruments Inc., Melville, NY) and confocal images were obtained with Leica TCS SP5 laser scanning confocal microscope (Leica Microsystems Inc., Buffalo Grove, IL), both at the IUB Light Microscopy Imaging Center of Indiana University. Additional information on antibodies and reagents used can be found in the supplemental methods.

Tissue protein extraction and Western blotting

Hair-free ventral skin was removed from KrP and KrP-ovex mice. Skin samples were snap-frozen using liquid nitrogen. Samples were digested using a 4% sodium dodecyl sulfate, protease and phosphatase inhibitor solution (1:100, #P8340 and #P0044 Sigma-Aldrich, St. Louis, MO). Mechanical lysis was carried out using an Eppendorf pestle followed by a QIAshredder column. The supernatant protein concentration was measured using the Pierce BCA Protein Assay Kit (#23227, Thermo Fisher Scientific, Waltham, MA). Samples were diluted to 0.35 µg/mL, 0.70 µg/mL or 1.40 µg/mL using the 4% sodium dodecyl sulfate solution and a Laemmli Buffer. Whole cell lysates from primary fibroblasts were prepared using RIPA buffer and were simultaneously monitored by blotting for ESR1, PSMAD, SMAD, and tubulin as loading control to determine that increased estrogen receptor levels were correlated with reduced Tgfb1 signaling in vitro. Western blotting was carried out as previously described (Nickerson, 2013). Additional information on antibodies and reagents used can be found in the supplemental methods.

qRT-PCR

Total RNA was isolated from sorted cells and/or tissues as previously described (Wu 2014) using RNeasy Mini Kit (74104, 74106, QIAGEN, Valencia CA) or RNeasy Micro Kit (74004, QIAGEN, Valencia CA) with on-column DNase I treatment according to manufacturer's instruction. 1µg of total RNA was reverse transcribed using SuperScript III First-Strand Synthesis SuperMix Kit (18080400, Thermo Scientific, Rockford IL) to generate cDNA. 40 ng of cDNA was used for qRT-PCR performed on a CFX Connect Real-Time system (BIO-RAD, Hercules CA) using iTaq Universal SYBR Green Supermix (172-5124, BIO-RAD, Hercules CA). All results were normalized to GAPDH housekeeping gene using $\Delta\Delta C_T$ method. Primer sequences are available from (BIO-RAD, Hercules CA). Analysis was performed on triplicates from samples of cDNA from 5 animals. Analyses were repeated twice with independent source RNA

BrdU incorporation

Proliferation was assessed by BrdU incorporation through intraperitoneal injection four hours prior to tissue harvest. A stock solution of 20 mg/mL of BrdU (5-Bromo-2'-deoxyuridine) (B5002, Sigma-Aldrich, St. Louis, MO) in 0.9% saline was prepared and stored in -20°C until use. 1 mg of BrdU was injected per 100 g body weight of the mice (Wu et al., 2015).

Statistics

Unless indicated, all *in vivo* data were presented as mean ± SEM from at least 3 replicates from three to six individual animals. All *in vitro* data were presented as mean ± SD of triplicate measurements of three independent replicates for a single

experiment. Experiments were repeated at least twice. Comparisons was evaluated by Student's t-test using GraphPad Prism, version 5.0 (GraphPad Software, Inc., La Jolla, CA), a P-value < 0.05 was considered to be significant. The genome-wide analysis was carried out using Partek Genomic Suite, version 6.5 (Partek Inc., St. Louis, MO).

Conflict of interest

The authors state no conflict of interest.

Acknowledgements

The microarray studies were carried out using the facilities of the Center for Medical Genomics at Indiana University School of Medicine supported in part by the Indiana Genomics Initiative at Indiana University (INGEN® and the Lilly Endowment, Inc.). We are thankful to Jeanette McClintick for the initial analysis of Micro Array data sets. We are grateful to Sue Childress for the blocking and serial sectioning of samples. We are grateful to Christiane Hassel at the IU Bloomington Flow Cytometry Core Facility supported by the Indiana CTSI. This work was supported by Indiana University School of Medicine Research Enhancement Grant to JF. HJW was supported by the Medical Sciences, Duan and Eunice Dahl Wright Scholarship. MVP is supported by the NIH NIAMS grants R01-AR067273, R01-AR069653, Edward Mallinckrodt Jr. Foundation grant and Pew Charitable Trust grant.

Author Contributions

HJW, ABG, DFS, CDO, ST, SK and JF designed the experiments. HJW, DFS, ST, SK, CDO, LS, and JF performed the experiments. HJW, JF, JDIII, MVP, SK, and JWO analyzed the data and HJW, MVP, SK, and JF wrote the manuscript.

References

Abdalkhani, A., Sellers, R., Gent, J., Wulitich, H., Childress, S., Stein, B., Boissy, R.E., Wysolmerski, J.J., and Foley, J. (2002). Nipple connective tissue and its development: insights from the K14-PTHrP mouse. Mech Dev *115*, 63-77.

Billingham, R.E., and Silvers, W.K. (1967). Studies on the conservation of epidermal specificies of skin and certain mucosas in adult mammals. The Journal of experimental medicine *125*, 429-446.

Bocchinfuso, W.P., and Korach, K.S. (1997). Mammary gland development and tumorigenesis in estrogen receptor knockout mice. Journal of mammary gland biology and neoplasia *2*, 323-334.

Botchkarev, V.A., Botchkareva, N.V., Roth, W., Nakamura, M., Chen, L.H., Herzog, W., Lindner, G., McMahon, J.A., Peters, C., Lauster, R.*, et al.* (1999). Noggin is a mesenchymally derived stimulator of hair-follicle induction. Nat Cell Biol *1*, 158-164.

Botchkarev, V.A., Botchkareva, N.V., Sharov, A.A., Funa, K., Huber, O., and Gilchrest, B.A. (2002). Modulation of BMP signaling by noggin is required for induction of the secondary (nontylotrich) hair follicles. The Journal of investigative dermatology *118*, 3-10.

Candille, S.I., Van Raamsdonk, C.D., Chen, C., Kuijper, S., Chen-Tsai, Y., Russ, A., Meijlink, F., and Barsh, G.S. (2004). Dorsoventral patterning of the mouse coat by Tbx15. PLoS Biol *2*, E3.

Chang, H.Y., Chi, J.T., Dudoit, S., Bondre, C., van de Rijn, M., Botstein, D., and Brown, P.O. (2002). Diversity, topographic differentiation, and positional memory in human fibroblasts. Proceedings of the National Academy of Sciences of the United States of America *99*, 12877-12882.

Cherlet, T., and Murphy, L.C. (2007). Estrogen receptors inhibit Smad3 transcriptional activity through Ap-1 transcription factors. Mol Cell Biochem *306*, 33-42.

Chi, W., Wu, E., and Morgan, B.A. (2013). Dermal papilla cell number specifies hair size, shape and cycling and its reduction causes follicular decline. Development *140*, 1676-1683.

Clavel, C., Grisanti, L., Zemla, R., Rezza, A., Barros, R., Sennett, R., Mazloom, A.R., Chung, C.Y., Cai, X., Cai, C.L.*, et al.* (2012). Sox2 in the dermal papilla niche controls hair growth by fine-tuning BMP signaling in differentiating hair shaft progenitors. Dev Cell *23*, 981-994.

Colletta, A.A., Wakefield, L.M., Howell, F.V., van Roozendaal, K.E., Danielpour, D., Ebbs, S.R., Sporn, M.B., and Baum, M. (1990). Anti-oestrogens induce the secretion of active transforming growth factor beta from human fetal fibroblasts. British journal of cancer *62*, 405-409.

Collins, C.A., Kretzschmar, K., and Watt, F.M. (2011). Reprogramming adult dermis to a neonatal state through epidermal activation of beta-catenin. Development *138*, 5189-5199.

Cunha, G.R., Young, P., Hom, Y.K., Cooke, P.S., Taylor, J.A., and Lubahn, D.B. (1997). Elucidation of a role for stromal steroid hormone receptors in mammary gland growth and development using tissue recombinants. Journal of mammary gland biology and neoplasia *2*, 393-402.

Dhouailly, D., and Oftedal, O.T. (2016). Integument and associated integumentary appendages. In Kaufmann's Atlas of Mouse Development with Coronal Sections R.B.J. Baldock, Davidson, D. Morriss-Kay, G. , ed. (Elsevier/Academic Press), pp. 147-164.

Dhouailly, D., Prin, F., Kanzler, B., and Viallet, J. (1998). Variations of Cutaneous Apendages: regional Specification and Cross-Species Signals. In Molecular Basis of Epithelial Appendage Morphogenesis, C. Cheng-Ming, ed. (Austin Texas: R.G. Landes Co.), pp. 45-56.

Driskell, R.R., Lichtenberger, B.M., Hoste, E., Kretzschmar, K., Simons, B.D., Charalambous, M., Ferron, S.R., Herault, Y., Pavlovic, G., Ferguson-Smith, A.C., *et al.* (2013). Distinct fibroblast lineages determine dermal architecture in skin development and repair. Nature *504*, 277-281.

Driskell, R.R., and Watt, F.M. (2015). Understanding fibroblast heterogeneity in the skin. Trends in cell biology *25*, 92-99.

Dunbar, M.E., Dann, P.R., Robinson, G.W., Hennighausen, L., Zhang, J.P., and Wysolmerski, J.J. (1999). Parathyroid hormone-related protein signaling is necessary for sexual dimorphism during embryonic mammary development. Development *126*, 3485-3493.

Dunbar, M.E., and Wysolmerski, J.J. (1999). Parathyroid hormone-related protein: a developmental regulatory molecule necessary for mammary gland development. Journal of mammary gland biology and neoplasia *4*, 21-34.

Eastwood, J., Offutt, C., Menon, K., Keel, M., Hrncirova, P., Novotny, M.V., Arnold, R., and Foley, J. (2007). Identification of markers for nipple epidermis: changes in expression during pregnancy and lactation. Differentiation; research in biological diversity *75*, 75-83.

Enshell-Seijffers, D., Lindon, C., Kashiwagi, M., and Morgan, B.A. (2010). beta-catenin activity in the dermal papilla regulates morphogenesis and regeneration of hair. Developmental cell *18*, 633-642.

Foley, J., Dann, P., Hong, J., Cosgrove, J., Dreyer, B., Rimm, D., Dunbar, M., Philbrick, W., and Wysolmerski, J. (2001). Parathyroid hormone-related protein maintains mammary epithelial fate and triggers nipple skin differentiation during embryonic breast development. Development *128*, 513-525.

Foley, J., Longely, B.J., Wysolmerski, J.J., Dreyer, B.E., Broadus, A.E., and Philbrick, W.M. (1998). PTHrP regulates epidermal differentiation in adult mice. The Journal of investigative dermatology *111*, 1122-1128.

Fu, J., and Hsu, W. (2013). Epidermal Wnt controls hair follicle induction by orchestrating dynamic signaling crosstalk between the epidermis and dermis. The Journal of investigative dermatology *133*, 890-898.

Habermann, E.B., Abbott, A., Parsons, H.M., Virnig, B.A., Al-Refaie, W.B., and Tuttle, T.M. (2010). Are mastectomy rates really increasing in the United States? Journal of clinical oncology : official journal of the American Society of Clinical Oncology *28*, 3437-3441.

Hens, J.R., Dann, P., Zhang, J.P., Harris, S., Robinson, G.W., and Wysolmerski, J. (2007). BMP4 and PTHrP interact to stimulate ductal outgrowth during embryonic mammary development and to inhibit hair follicle induction. Development *134*, 1221-1230.

Hewitt, S.C., Li, Y., Li, L., and Korach, K.S. (2010). Estrogen-mediated regulation of Igf1 transcription and uterine growth involves direct binding of estrogen receptor alpha to estrogen-responsive elements. J Biol Chem *285*, 2676-2685.

Hiremath, M., Dann, P., Fischer, J., Butterworth, D., Boras-Granic, K., Hens, J., Van Houten, J., Shi, W., and Wysolmerski, J. (2012). Parathyroid hormone-related protein activates Wnt signaling to specify the embryonic mammary mesenchyme. Development *139*, 4239-4249.

Jahoda, C.A., Horne, K.A., and Oliver, R.F. (1984). Induction of hair growth by implantation of cultured dermal papilla cells. Nature *311*, 560-562.

Jahoda, C.A., Reynolds, A.J., and Oliver, R.F. (1993). Induction of hair growth in ear wounds by cultured dermal papilla cells. The Journal of investigative dermatology *101*, 584-590.

Javed, A., and Lteif, A. (2013). Development of the human breast. Seminars in plastic surgery *27*, 5-12.

Kalluri, R., and Zeisberg, M. (2006). Fibroblasts in cancer. Nature reviews Cancer *6*, 392-401.

Knabbe, C., Lippman, M.E., Wakefield, L.M., Flanders, K.C., Kasid, A., Derynck, R., and Dickson, R.B. (1987). Evidence that transforming growth factor-beta is a hormonally regulated negative growth factor in human breast cancer cells. Cell *48*, 417-428.

Koyama, S., Wu, H.J., Easwaran, T., Thopady, S., and Foley, J. (2013). The nipple: a simple intersection of mammary gland and integument, but focal point of organ function. Journal of mammary gland biology and neoplasia *18*, 121-131.

Lapidus, R.G., Nass, S.J., and Davidson, N.E. (1998). The loss of estrogen and progesterone receptor gene expression in human breast cancer. Journal of mammary gland biology and neoplasia *3*, 85-94.

Lee, L.F., Jiang, T.X., Garner, W., and Chuong, C.M. (2011). A simplified procedure to reconstitute hair-producing skin. Tissue engineering Part C, Methods *17*, 391-400.

Lichti, U., Anders, J., and Yuspa, S.H. (2008). Isolation and short-term culture of primary keratinocytes, hair follicle populations and dermal cells from newborn mice and keratinocytes from adult mice for in vitro analysis and for grafting to immunodeficient mice. Nature protocols *3*, 799-810.

Lichti, U., Scandurro, A.B., Kartasova, T., Rubin, J.S., LaRochelle, W., and Yuspa, S.H. (1995). Hair follicle development and hair growth from defined cell populations grafted onto nude mice. The Journal of investigative dermatology *104*, 43S-44S.

Lichti, U., Weinberg, W.C., Goodman, L., Ledbetter, S., Dooley, T., Morgan, D., and Yuspa, S.H. (1993). In vivo regulation of murine hair growth: insights from grafting defined cell populations onto nude mice. The Journal of investigative dermatology *101*, 124S-129S.

Liu, X., Alexander, V., Vijayachandra, K., Bhogte, E., Diamond, I., and Glick, A. (2001). Conditional epidermal expression of TGFbeta 1 blocks neonatal lethality but causes a reversible hyperplasia and alopecia. Proceedings of the National Academy of Sciences of the United States of America *98*, 9139-9144.

Mackenzie, I.C., and Hill, M.W. (1981). Maintenance of regionally specific patterns of cell proliferation and differentiation in transplanted skin and oral mucosa. Cell and tissue research *219*, 597-607.

Mackenzie, I.C., and Hill, M.W. (1984). Connective tissue influences on patterns of epithelial architecture and keratinization in skin and oral mucosa of the adult mouse. Cell and tissue research *235*, 551-559.

Mahler, B., Gocken, T., Brojan, M., Childress, S., Spandau, D.F., and Foley, J. (2004). Keratin 2e: a marker for murine nipple epidermis. Cells, tissues, organs *176*, 169-177.

Mauviel, A. (2009). Transforming growth factor-beta signaling in skin: stromal to epithelial cross-talk. The Journal of investigative dermatology *129*, 7-9.

McCormack, J.T., and Greenwald, G.S. (1974). Progesterone and oestradiol-17beta concentrations in the peripheral plasma during pregnancy in the mouse. J Endocrinol *62*, 101-107.

Menz, H.B., Zammit, G.V., and Munteanu, S.E. (2007). Plantar pressures are higher under callused regions of the foot in older people. Clinical and experimental dermatology *32*, 375-380.

Millar, S.E. (2002). Molecular mechanisms regulating hair follicle development. The Journal of investigative dermatology *118*, 216-225.

Morgan, B.A. (2014). The dermal papilla: an instructive niche for epithelial stem and progenitor cells in development and regeneration of the hair follicle. Cold Spring Harb Perspect Med *4*, a015180.

Moyer, H.R., Ghazi, B., Daniel, J.R., Gasgarth, R., and Carlson, G.W. (2012). Nipple-sparing mastectomy: technical aspects and aesthetic outcomes. Annals of plastic surgery *68*, 446-450.

Neifert, M., DeMarzo, S., Seacat, J., Young, D., Leff, M., and Orleans, M. (1990). The influence of breast surgery, breast appearance, and pregnancy-induced breast changes on lactation sufficiency as measured by infant weight gain. Birth *17*, 31-38.

Nickerson, N. (2013). Autocrine-Derived Epidermal Growth Factor Receptor Ligands Contribute to Recruitment of Tumor-Associated Macrophage
and Growth of Basal Breast Cancer Cells In Vivo.

Oftedal, O.T., and Dhouailly, D. (2013). Evo-devo of the mammary gland. Journal of mammary gland biology and neoplasia *18*, 105-120.

Oshimori, N., and Fuchs, E. (2012). Paracrine TGF-beta signaling counterbalances BMP-mediated repression in hair follicle stem cell activation. Cell stem cell *10*, 63-75.

Parkin, D.M., and Fernandez, L.M. (2006). Use of statistics to assess the global burden of breast cancer. The breast journal *12 Suppl 1*, S70-80.

Plikus, M.V. (2014). At the dawn of hair research - testing the limits of hair follicle regeneration. Exp Dermatol *23*, 314-315.

Quevedo, W.C., Jr., and Fleischmann, R.D. (1980). Developmental biology of mammalian melanocytes. The Journal of investigative dermatology *75*, 116-120.

Rendl, M., Lewis, L., and Fuchs, E. (2005). Molecular dissection of mesenchymal-epithelial interactions in the hair follicle. PLoS Biol *3*, e331.

Rendl, M., Polak, L., and Fuchs, E. (2008). BMP signaling in dermal papilla cells is required for their hair follicle-inductive properties. Genes & development *22*, 543-557.

Rinn, J.L., Bondre, C., Gladstone, H.B., Brown, P.O., and Chang, H.Y. (2006). Anatomic demarcation by positional variation in fibroblast gene expression programs. PLoS genetics *2*, e119.

Rinn, J.L., Wang, J.K., Allen, N., Brugmann, S.A., Mikels, A.J., Liu, H., Ridky, T.W., Stadler, H.S., Nusse, R., Helms, J.A.*, et al.* (2008). A dermal HOX transcriptional program regulates site-specific epidermal fate. Genes & development *22*, 303-307.

Robertson, I.B., Horiguchi, M., Zilberberg, L., Dabovic, B., Hadjiolova, K., and Rifkin, D.B. (2015). Latent TGF-beta-binding proteins. Matrix biology : journal of the International Society for Matrix Biology *47*, 44-53.

Sakakura, T. (1987). Mammary embryogenesis. In The Mammary gland : development, regulation, and function, M.C. Neville, and C.W. Daniel, eds. (New York: Plenum Press), pp. 37-66.

Sakakura, T., Kusano, I., Kusakabe, M., Inaguma, Y., and Nishizuka, Y. (1987). Biology of mammary fat pad in fetal mouse: capacity to support development of various fetal epithelia in vivo. Development *100*, 421-430.

Schweizer, J. (1993). Murine epidermal keratins. In Molecular biology of the skin : the keratinocyte, M. Darmon, and M.L. Blumenberg, eds. (San Diego: Academic Press), pp. 33-78.

Schweizer, J., Winter, H., Hill, M.W., and Mackenzie, I.C. (1984). The keratin polypeptide patterns in heterotypically recombined epithelia of skin and mucosa of adult mouse. Differentiation; research in biological diversity *26*, 144-153.

Sennett, R., and Rendl, M. (2012). Mesenchymal-epithelial interactions during hair follicle morphogenesis and cycling. Semin Cell Dev Biol *23*, 917-927.

Shaikh-Naidu, N., Preminger, B.A., Rogers, K., Messina, P., and Gayle, L.B. (2004). Determinants of aesthetic satisfaction following TRAM and implant breast reconstruction. Annals of plastic surgery *52*, 465-470; discussion 470.

Sriram, G., Bigliardi, P.L., and Bigliardi-Qi, M. (2015). Fibroblast heterogeneity and its implications for engineering organotypic skin models in vitro. European journal of cell biology.

Szabowski, A., Maas-Szabowski, N., Andrecht, S., Kolbus, A., Schorpp-Kistner, M., Fusenig, N.E., and Angel, P. (2000). c-Jun and JunB antagonistically control cytokine-regulated mesenchymal-epidermal interaction in skin. Cell *103*, 745-755.

Tan, C.M., Chen, E.Y., Dannenfelser, R., Clark, N.R., and Ma'ayan, A. (2013). Network2Canvas: network visualization on a canvas with enrichment analysis. Bioinformatics *29*, 1872-1878.

VandeBerg, J.L., Williams-Blangero, S., and Tardif, S.D. (2009). The baboon in biomedical research (New York: Springer).

Weinberg, W.C., Goodman, L.V., George, C., Morgan, D.L., Ledbetter, S., Yuspa, S.H., and Lichti, U. (1993). Reconstitution of hair follicle development in vivo: determination of follicle formation, hair growth, and hair quality by dermal cells. The Journal of investigative dermatology *100*, 229-236.

Wu, H.J., Easwaran, T., Offutt, C.D., Elgar, R.L., Spandau, D.F., Koyama, S., and Foley, J. (2015). Expansion of specialized epidermis induced by hormonal state and mechanical strain. Mech Dev *136*, 73-86.

Wysolmerski, J.J., Broadus, A.E., Zhou, J., Fuchs, E., Milstone, L.M., and Philbrick, W.M. (1994). Overexpression of parathyroid hormone-related protein in the skin of transgenic mice interferes with hair follicle development. Proceedings of the National Academy of Sciences of the United States of America *91*, 1133-1137.

Wysolmerski, J.J., Philbrick, W.M., Dunbar, M.E., Lanske, B., Kronenberg, H., and Broadus, A.E. (1998). Rescue of the parathyroid hormone-related protein knockout mouse demonstrates that parathyroid hormone-related protein is essential for mammary gland development. Development *125*, 1285-1294.

Yamaguchi (1999). Regulation of K9 in nonpalmoplantar keratinocytes by.

Yamaguchi, Y., Itami, S., Watabe, H., Yasumoto, K., Abdel-Malek, Z.A., Kubo, T., Rouzaud, F., Tanemura, A., Yoshikawa, K., and Hearing, V.J. (2004). Mesenchymal-epithelial interactions in the skin: increased expression of dickkopf1 by palmoplantar fibroblasts inhibits melanocyte growth and differentiation. The Journal of cell biology *165*, 275-285.

Yamaguchi, Y., Morita, A., Maeda, A., and Hearing, V.J. (2009). Regulation of skin pigmentation and thickness by Dickkopf 1 (DKK1). J Investig Dermatol Symp Proc *14*, 73-75.

Yamaguchi, Y., Passeron, T., Hoashi, T., Watabe, H., Rouzaud, F., Yasumoto, K., Hara, T., Tohyama, C., Katayama, I., Miki, T., *et al.* (2008). Dickkopf 1 (DKK1) regulates skin pigmentation and thickness by affecting Wnt/beta-catenin signaling in keratinocytes. FASEB journal : official publication of the Federation of American Societies for Experimental Biology *22*, 1009-1020.

Yang, C.C., and Cotsarelis, G. (2010). Review of hair follicle dermal cells. Journal of dermatological science *57*, 2-11.

Yokota, T., Oritani, K., Garrett, K.P., Kouro, T., Nishida, M., Takahashi, I., Ichii, M., Satoh, Y., Kincade, P.W., and Kanakura, Y. (2008). Soluble frizzled-related protein 1 is estrogen inducible in bone marrow stromal cells and suppresses the earliest events in lymphopoiesis. Journal of immunology *181*, 6061-6072.

Zingg, H.H., Grazzini, E., Breton, C., Larcher, A., Rozen, F., Russo, C., Guillon, G., and Mouillac, B. (1998). Genomic and non-genomic mechanisms of oxytocin receptor regulation. Adv Exp Med Biol *449*, 287-295.

Figures

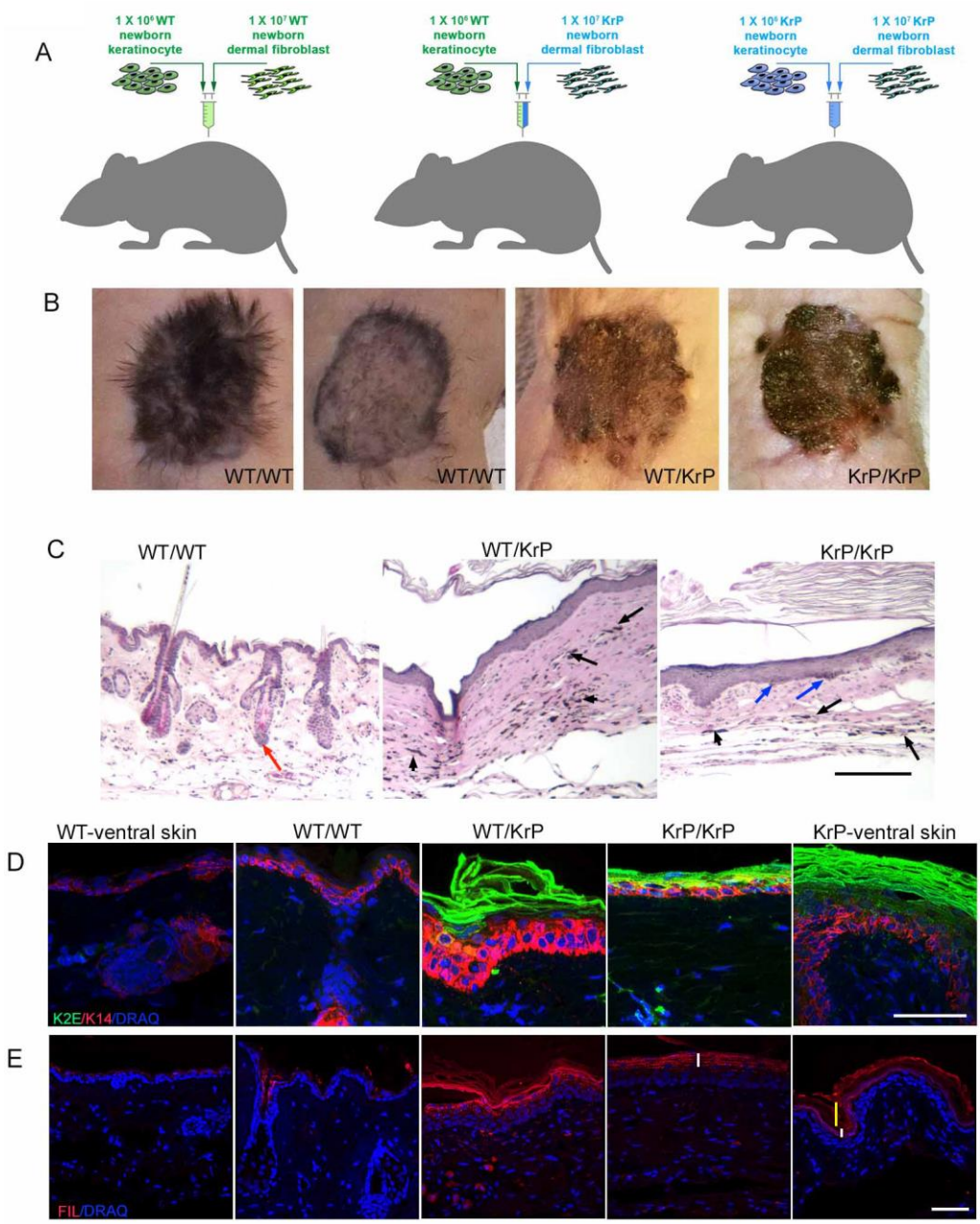

Figure 1. Fibroblasts from nipple-like skin are sufficient to induce specialized epidermis. (A) Schematic outline of grafting experiment. **(B)** Hairless pigmented nipple-like skin was present in three month-old WT/KrP and KrP/KrP grafts on the

dorsum of BALB/c *Foxn1*$^{nu/nu}$ host mice. WT/WT grafts produced pigmented hair, but hair clipping revealed non-pigmented skin underneath. **(C)** H&E staining of grafts. Black arrows point at pigmented cells in the dermis of KrP/KrP and WT/KrP grafts. Occasionally pigment could be observed in the epidermis of the nipple-like grafts (blue arrows), whereas pigment was mainly confined to hair follicles in WT/WT grafts (red arrow). Scale bar: 400 μM. (**D**) K2e and K14 immunostaining. WT/KrP and KrP/KrP grafts stain for K2e as does the KrP ventral skin. Scale bar; 50 μM. (**E**) Filaggrin immunostaining. Multiple suprabasal layers in WT/KrP and KrP/KrP grafts and KrP ventral skin stain for filaggrin, compared to minimal labeling in the WT/WT grafts and intact WT skin. The white vertical bar indicates the granular layer and the yellow the cornified layer. Note the cornified layer is lost in KrP/KrP graft due to antigen retrieval. Scale bar: 50 μm. WT: wild-type; KrP: *K14-PTHrP* transgenic mice; K2E: Keratin 2e, K14: Keratin 14; Fil: filaggrin; DRAQ: nuclei.

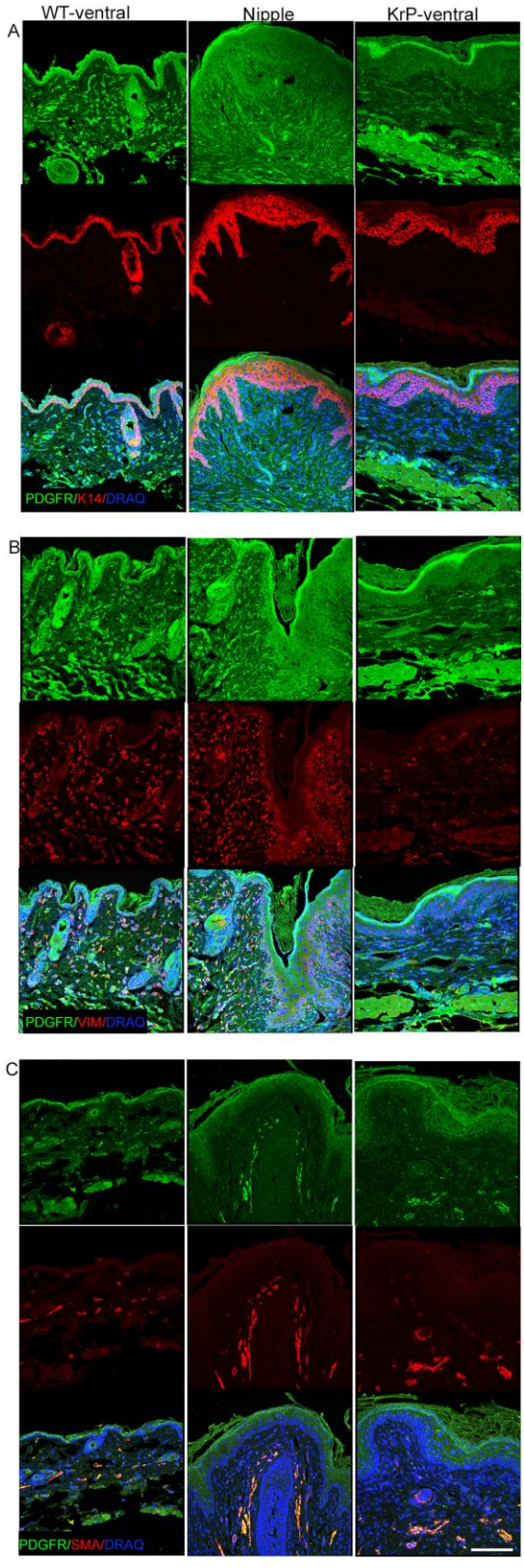

Figure 2. Pdgfrα expression pattern in ventral skin and nipple tissue. Co-staining of ventral skin from WT mice (left), KrP mice (right) and WT virgin nipple (center) for Pdgfrα (platelet-derived growth factor receptor alpha, green), and **(A)** K14 (keratin-14, red), **(B)** Vim (vimentin, red) or **(C)** Sma (smooth muscle actin, red). Nuclei were counterstained blue with DRAQ5. Scale bar: 96.5 μm. Differential intensity for PDGFR staining among the sections reflects the use of different antibodies in A&B versus C. The intense labeling of the granular layer in the nipple and KrP samples of A&B is likely non-specific.

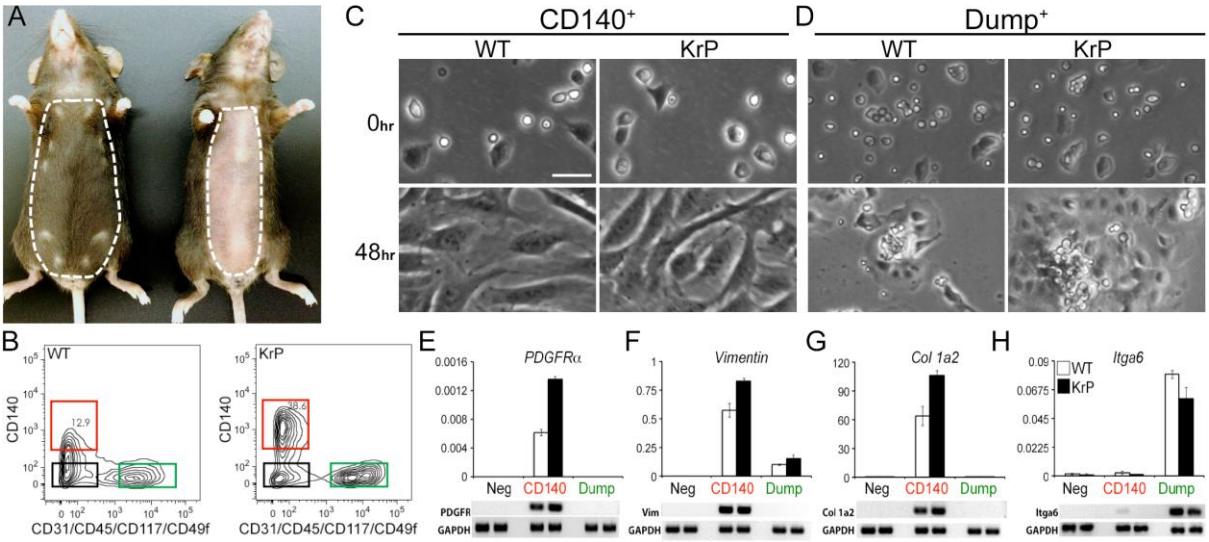

Figure 3. Pdgfrα labels mouse nipple fibroblast population. (A) Dotted outline marks ventral skin in either WT (left) or KrP mice (right) used as the source for fibroblasts. **(B)** FACS gating strategy used to isolate Pdgfrα^+ cells (fibroblasts, red box), dump-channel$^+$ cells (mix of cells marked for CD31$^+$, CD45$^+$, CD117$^+$ or CD49f$^+$, green box) and double-negative Pdgfrα$^-$/Dump-channel$^-$ cells (black box). **(C-D)** Appearance of cells in transient primary culture: sorted Pdgfrα$^+$ cells **(C)** and dump-channel$^+$ cells **(D).** Only Pdgfrα$^+$ cells display fibroblast morphology. Scale bar: 25 µm. **(E-H)** qRT-PCR for select genes in sorted cell populations. All target genes were normalized to *Gapdh*. Each bar represents the average of three independent experiments from five mice of each genotype (±s.d.).

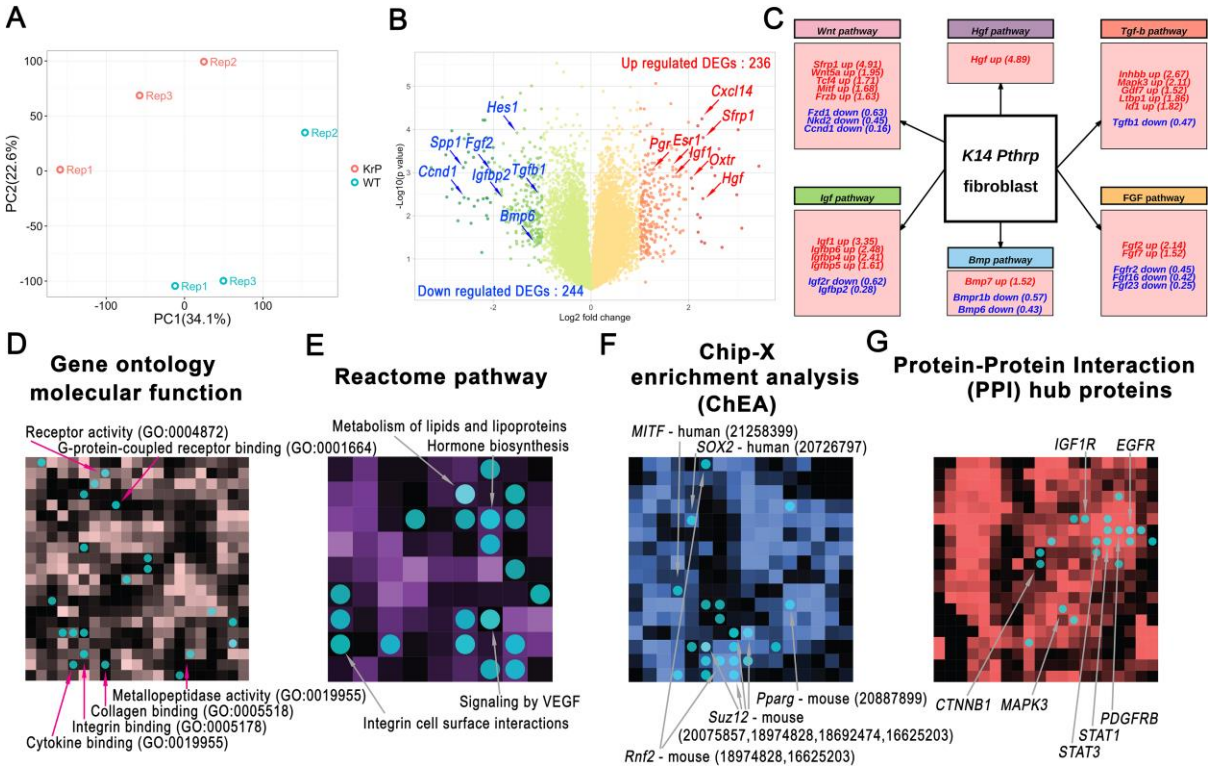

Figure 4. Bioinformatic comparison of KrP ventral fibroblasts with WT ventral fibroblasts. (A) Principal component analysis of KrP (red) *vs.* WT ventral fibroblasts (blue) reveals global gene expression differences between cells of distinct genotypes. Dots represent individual biological replicates. **(B)** Volcano plot shows the relationship between gene expression fold-changes and p-values across two genotypes. Red annotations mark differentially expressed genes (DEGs) upregulated in KrP ventral fibroblasts, while blue annotations mark downregulated DEGs. Positions for several up- and downregulated DEGs on the volcano plot are annotated. **(C)** Summary of DEGs classified by their signaling pathway identity, WNT, HGF, TGFβ, IGF, BMP and FGF. Red annotations identify DEGs upregulated in KrP ventral fibroblasts, while blue annotations identify downregulated DEGs. For each

gene, KrP *vs.* WT fold-change is provided. **(D-G)** Network2Canvas analyses for four gene-set libraries: Gene ontology molecular function **(D)**, Reactome pathway **(E)**, Chip-X enrichment analysis (ChEA) **(F)**, and Protein-protein interaction (PPI) hub proteins **(G).** Each canvas represents a specific gene-set library, where individual squares represent gene lists linked with gene-set library groups (or pathway gene groups). Square brightness is determined by its similarity to its eight neighbors. Each circle (blue) represents top 20 enriched pathways using KrP *vs.* WT DEGs within specific gene set library. Only relevant and statistically significant pathways are annotated here. Full lists of top 20 circles are in the Supplementary table 2.

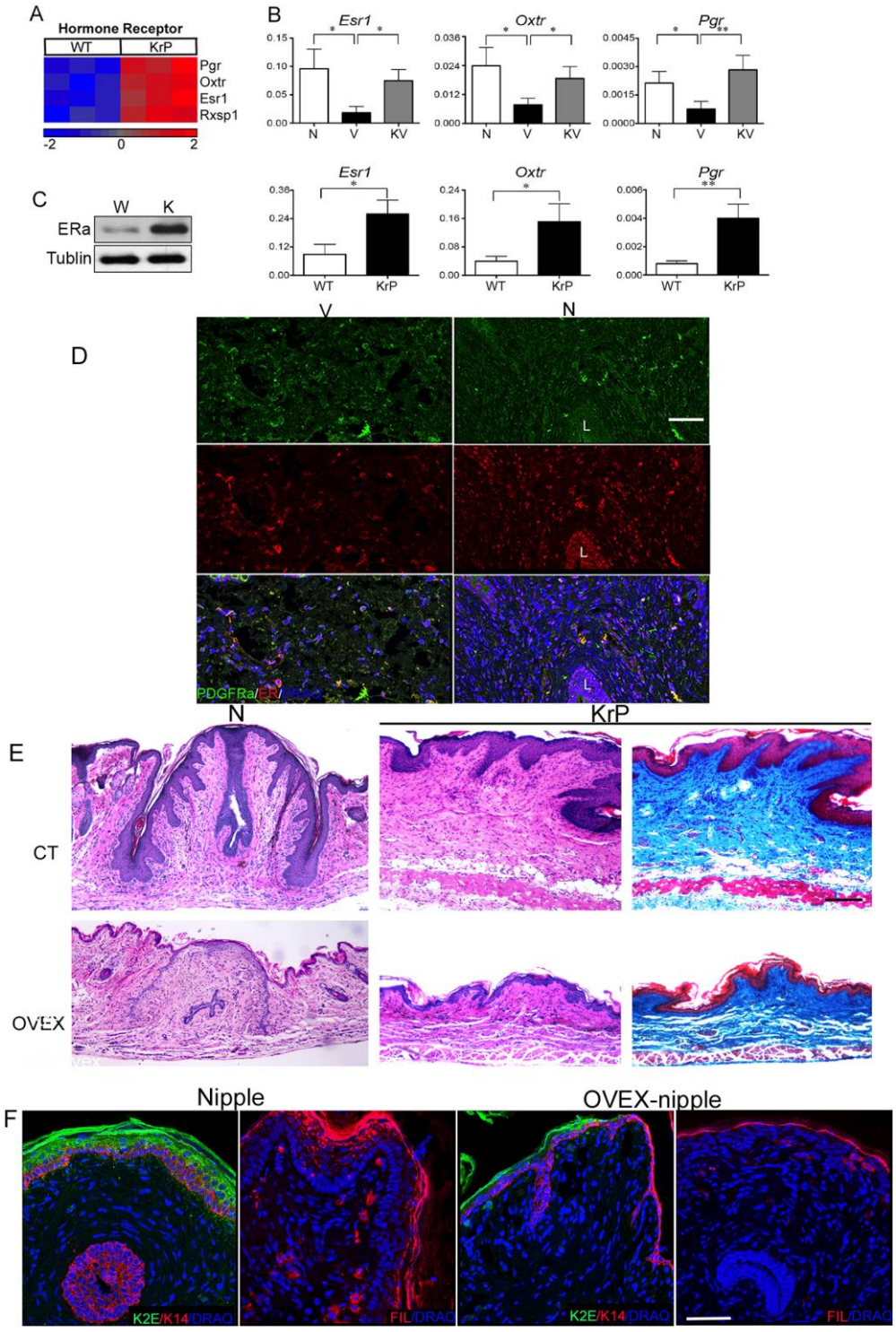

Figure 5. Estrogen receptor expression and the role of ovarian hormones in the nipple. (A) Heatmap representations of hormone receptors expression in KrP *vs.* WT fibroblasts in three independent experiments. **(B)** qRT-PCR for receptor gene levels in intact tissues and sorted fibroblasts. N: nipple of WT mouse; V: ventral skin

of WT mouse; KV: ventral skin of KrP mouse; WT: sorted WT ventral fibroblast; KrP: sorted KrP fibroblasts. *Esr1*: estrogen receptor alpha; *Oxtr*: oxytocin receptor; *Pgr*: progesterone receptor. **(C)** Western blot of cell extracts from cultured KrP and WT fibroblasts probed with anti-ERα antibody using purified fibroblast. The same protein extracts used in 6D were blotted in parallel and the same β-tublin blot serves as loading control. W: WT ventral fibroblasts; K: KrP fibroblasts. **(D)** Co-expression patterns of Pdgfrα (Green) and ERα (Red) in virgin WT mice. Nuclei were counterstained blue with DRAQ5. V: ventral skin; N: nipple; L: lactiferous duct. Scale bar: 60 μm. **(E)** Histology of WT nipples and KrP ventral skin from ovexed mice. H&E and Masson's trichrome stains demonstrate thinner epidermis and increased size of collagen bundles under ovexed conditions. Scale bar: 400 μm. **(F)** Epidermal marker expression in nipples from ovexed and control mice. Layers of K2e, filaggrin and K14 antibody labeled cells a markedly diminished under ovexed conditions. Scale bar: 50 μm.

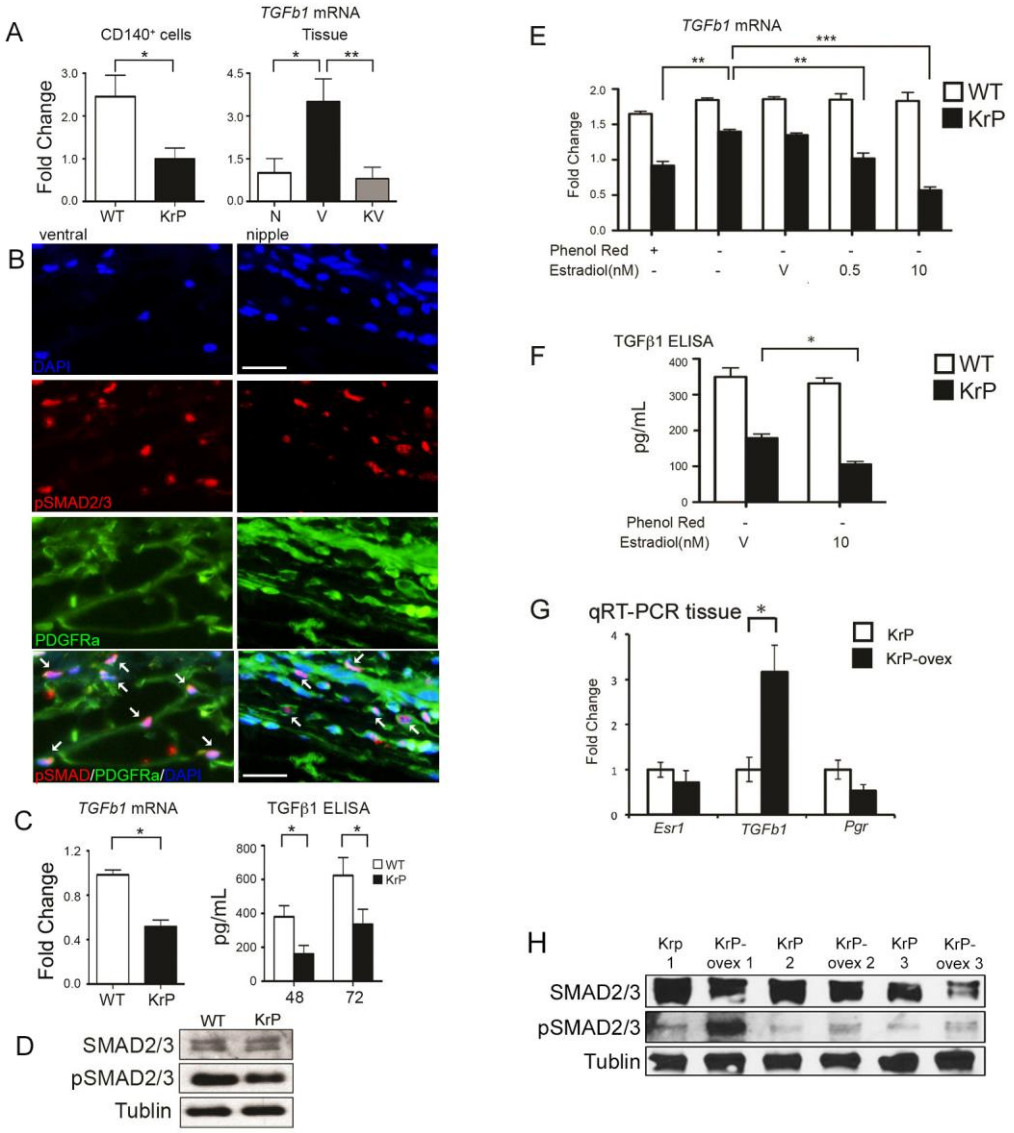

Figure 6. Estrogen signaling negatively regulates TGFβ signaling in nipple fibroblasts. (A) *Tgfb1* expression in CD140^{+} sorted fibroblasts and intact tissues. N: nipple of WT mouse; V: ventral skin of WT mouse; KV: ventral skin of KrP mouse. Expression was normalized to *Gapdh*. **(B)** Co-staining for Pdgfrα (green) and pSmad2/3 (red) of ventral dermis and nipples of virgin WT mouse. Nuclei were counterstained with DAPI (blue). Scale bar: 25 μm. **(C)** *Tgfb1* expression levels in

cultured fibroblasts (by qRT-PCR) and secreted levels of Tgfb1 in culture media of purified fibroblasts (by ELISA). *P < 0.05. Measurements were collected from three different cultures and performed in triplicate. **(D)** Western blot of purified fibroblasts probed with Smad2/3 and pSmad2/3 antibodies. The same protein extracts used in 5C were blotted in parallel and the same β-tublin blot serves as loading control. **(E)** Relative *Tgfb1* levels in primary cultured fibroblasts treated with or without Estradiol treatment. Expression of *Tgfb1* was measured by qRT-PCR and normalized to *Gapdh*. Each bar represents the average of three independent experiments (±s.d.). **P < 0.01, ***P < 0.001. **(F)** ELISA measurements of secreted Tgfb1 in culture media harvested from primary cultured fibroblast with or without Estradiol treatment. Each bar represents the average ±s.d. of triplicate cultures within single experiment. The experiment was repeated twice with similar results. *P < 0.05. **(G)** Relative *Esr1, Tgfb1 and Pr* mRNA levels in ventral skin of ovexed as compared to age-matched control KrP mice. *P < 0.05. **(H)** Western blot of extracts from intact ventral tissues from ovexed and control KrP mice probed with Smad2/3 and pSmad2/3 antibodies. β-tublin used as loading control. *P < 0.05.

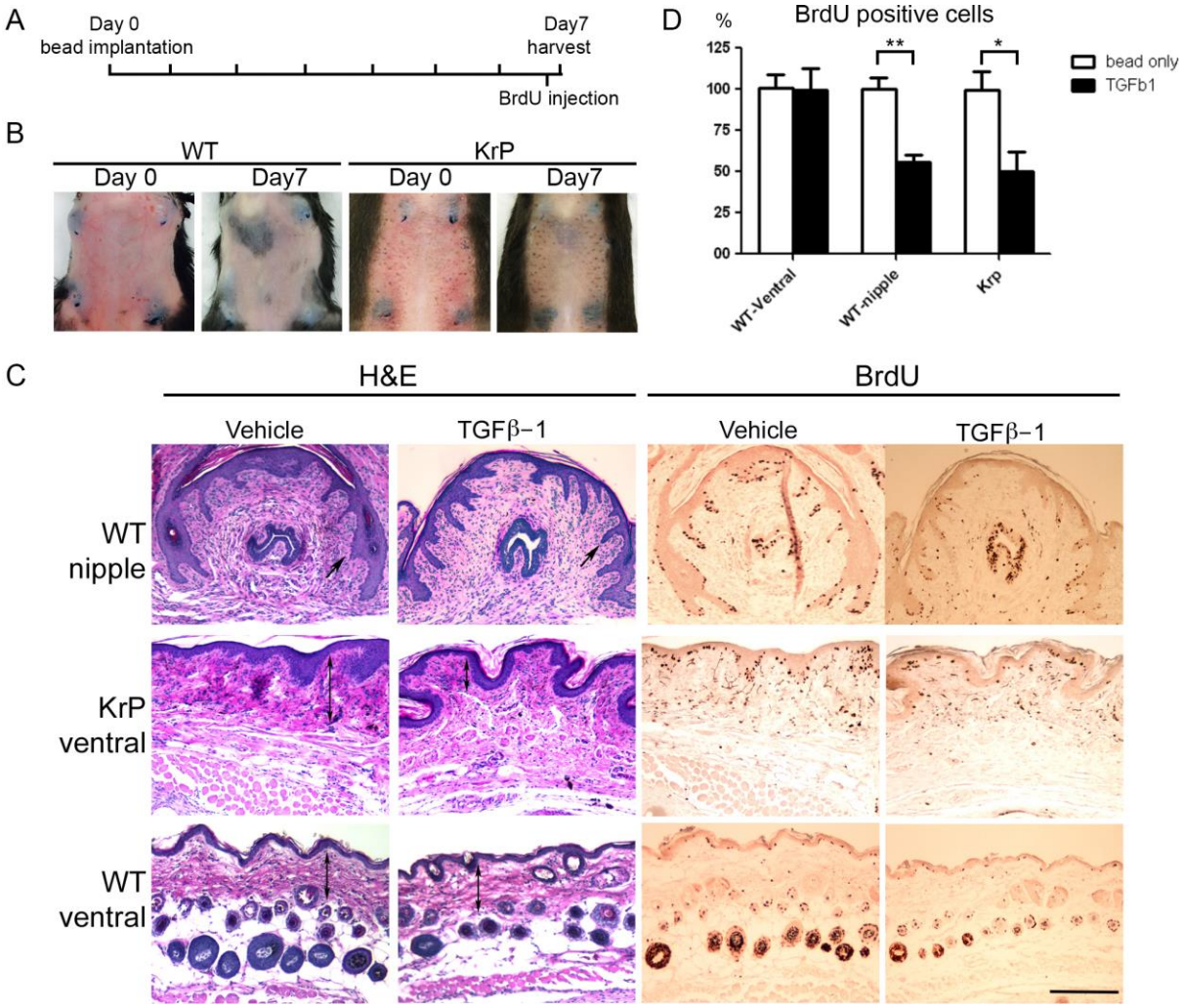

Figure 7. Sustained dermal activation of TGFβ signaling induces collagen remodeling and epidermal hypoplasia in the nipple. (A) Affi-gel blue beads with or without 0.2 µg of recombinant Tgfb1 were injected intradermally into KrP ventral skin or WT nipple. Samples were collected 7 days post-implantation. BrdU was injected 4 hours prior to sample collection. **(B)** Affi-gel blue beads remain at the site of injection 7 days post implantation. **(C)** Bead-treated samples were stained for H&E and BrdU. Scale bar: 60 µm. Quantification of BrdU-positive keratinocytes relative to the length of basal epidermis is shown in **(D).**

Supplemental Methods

Isolation of adult fibroblasts

The collagenase solution contained 1.25 mg/ml Collagenase type I (Gibco Thermo Fisher Scientific, Waltham, MA), 0.5 mg/ml Collagenase type II (Worthington Biochemical Co., Lakewood, NJ), 0.5 mg/ml Collagenase type IV (Sigma-Aldrich, St. Louis, MO), and 50 U/ml DNase I (Worthington Biochemical Co., Lakewood, NJ) in DMEM media at 37°C for one hour. The preparations were then passed through blunt-end needles several times to mechanically dissociate dermis before filtering the mixture through a 70 μm strainer.

Note that the ventral dermis of WT mice would contain a very small number of nipple fibroblasts.

qRT-PCR

Total RNA was isolated using RNeasy Mini Kit (74104, 74106, QIAGEN, Valencia, CA) or RNeasy Micro Kit (74004, QIAGEN, Valencia, CA) with on-column DNase I treatment according to manufacturer's instruction. 1 μg of total RNA was reverse-transcribed using SuperScript III First-Strand Synthesis SuperMix Kit (18080400, Thermo Fisher Scientific, Waltham, MA) to generate cDNA. 40 ng of cDNA was used for qRT-PCR performed on a CFX Connect Real-Time system (BIO-RAD, Hercules, CA) using iTaq Universal SYBR Green Supermix (172-5124, BIO-RAD, Hercules, CA).

Statistics

Histology and immunofluorescence

Samples were collected, fixed and sectioned as previously described (Wu et al., 2015). The following primary antibodies against the following proteins were used: vimentin (mouse monoclonal, ab28028, Abcam, Cambridge MA), smooth muscle actin 1:50 (mouse monoclonal, A2547, Sigma-Aldrich, St. Louis MO), cytokeratin 2e 1:500 (mouse monoclonal 10R-C166a, Fitzgerald, Acton, MA), Keratin 14 (rabbit polyclonal, 905301, BioLegend, San Diego, CA), filaggrin 1:5,000 (rabbit polyclonal, 905801, BioLegend, San Diego, CA), Pdgfrα 1:200 (goat polyclonal, AF1062, R&D systems, Minneapolis MN and C-9 Santa Cruz Biotechnology, Dallas, TX), Esr1 (rabbit polyclonal, HC-20, Santa Cruz Biotechnology, Dallas, TX), Smad2/3 (rabbit polyclonal, FL-425, Santa Cruz Biotechnology, Dallas, TX), pSmad2/3 1:200 (goat polyclonal, sc-11769, Santa Cruz Biotechnology, Dallas, TX). Secondary antibodies were used at 1:200 to 1:500 dilution (Jackson Immuno Research Laboratories Inc., West Grove, PA), including Alexa-Fluor 488 or 647- conjugated goat anti-rabbit or anti-mouse IgG. Nucleus staining was conducted using DAPI (D1306, Thermo Fisher Scientific, Waltham, MA) or Draq5 (62251, Thermo Fisher Scientific, Waltham, MA).

Western Blotting

The following primary antibodies were used: ERa (rabbit polyclonal, HC-20, Santa Cruz Biotechnology, Dallas, TX), Smad2/3 (rabbit polyclonal, FL-425, Santa Cruz Biotechnology, Dallas, TX), pSmad2/3 (sc-11769R, Santa Cruz Biotechnology, Dallas, TX). For the tissue analysis the following antibodies were

used: β-tubulin 1:125 (mouse monoclonal, E7-s, Developmental Studies Hybridoma Bank, Iowa City IA), p-Smad2/3 (Ser 423/425) 1:100 (rabbit polyclonal, sc-11769, Santa Cruz Biotechnology, Dallas, TX), Smad2/3 (C-8) 1:200 (mouse monoclonal, sc-133098, Santa Cruz Biotechnology, Dallas, TX).

Supplementary Tables

Supplementary table 1. Microarray gene expression data and analysis. generated from sorted Pdgfrα-positive ventral KrP and WT fibroblasts. Tab 1, raw gene expression data; tab 2, list of up-regulated genes; tab 3, list of down-regulated genes; tab 4, select signaling pathway genes; tab 5, reference signaling pathway gene list.

Click here to Download Table S1

Supplementary table 2. Differential gene expression analysis on Pdgfrα-positive ventral KrP and WT fibroblasts using Network2Canvas platform. Individual tabs contains lists of enriched terms within given gene networks.

Click here to Download Table S2

Supplemental Figures

Supplementfig1

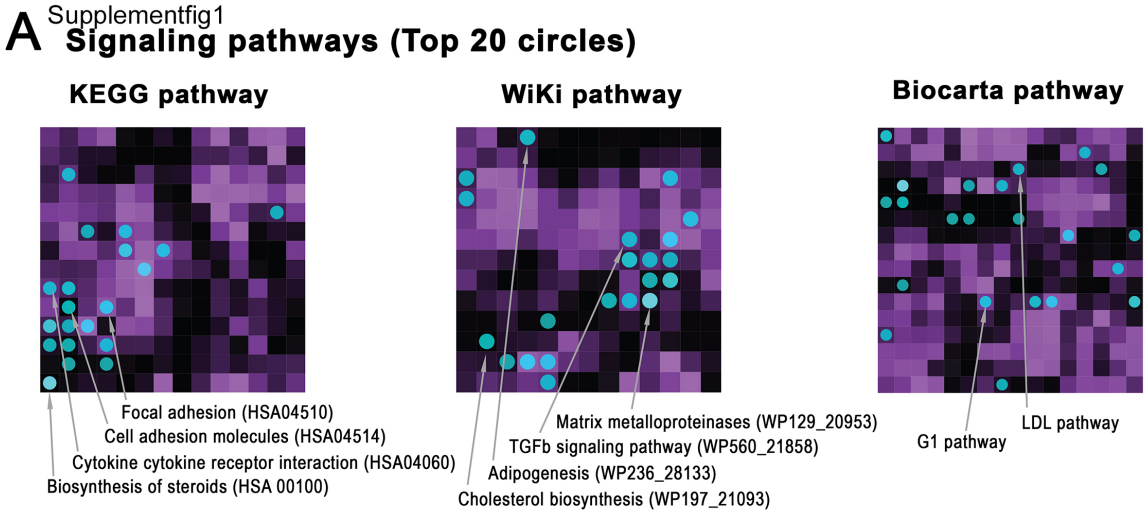

Supplemental Figures and Legends:

Supplemental figure 1. Network2Canvas analysis of KrP *vs.* WT ventral fibroblasts for seven gene-set libraries. Signaling pathways **(A),** Transcription **(B),** Kinase enrichment analysis **(C),** and Gene ontology and Cancer cell line encyclopedia **(D).** Each canvas represents a specific gene-set library, where each square represents a gene list linked with a gene-set library group. Square brightness is determined by its similarity to its eight neighbors. Each circle (blue) represents top 20 enriched pathways using KrP *vs.* WT DEGs within specific gene set library. Only relevant and statistically significant pathways are selectively annotated. Also see Supplementary tables 1 and 2.

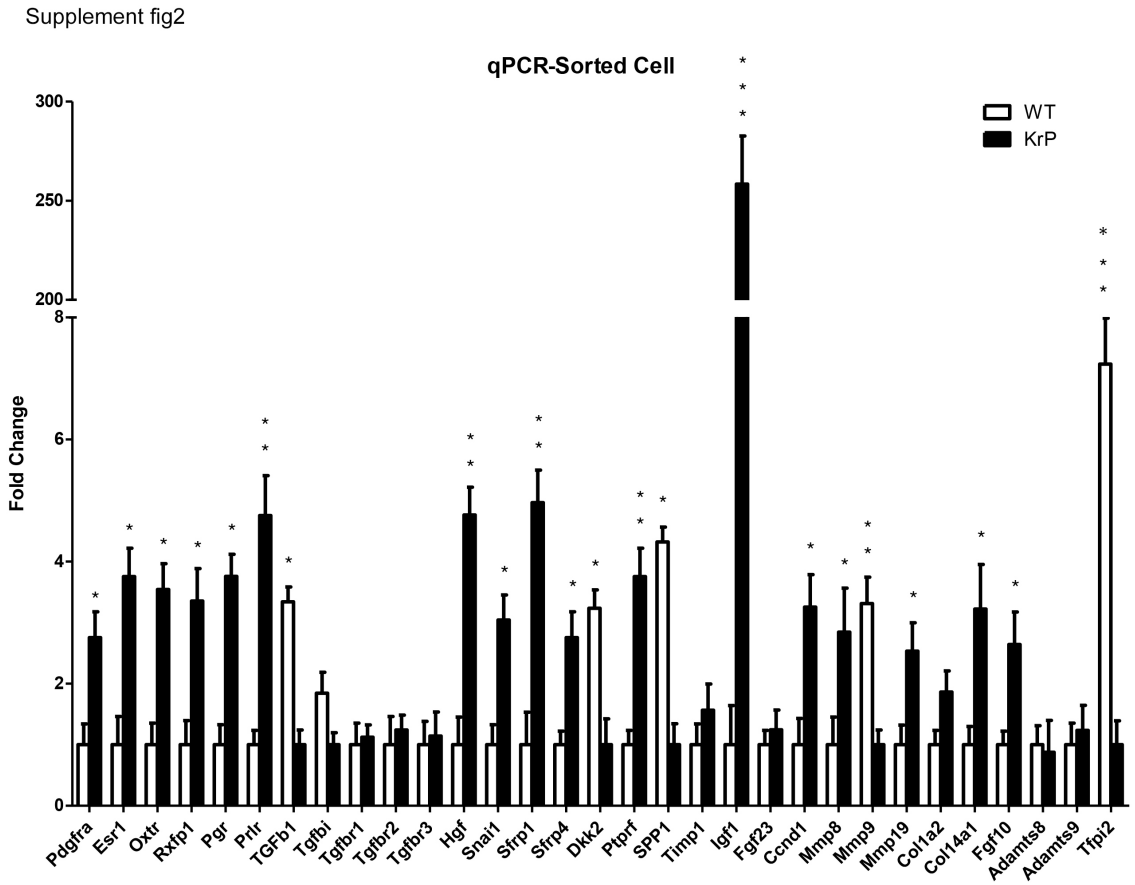

Supplemental Figure 2. Confirmation of select differentially expressed genes by qRT-PCR using RNA from sorted cells. The differential expression of 30 transcripts (20 increased, 6 decreased and 4 unchanged in KrP relative to WT fibroblasts), many of which are part of the pathways identified by the Ingenuity and GO term analysis, was confirmed by qRT-PCR (Fig. S2). Of the transcripts evaluated, all with the exception of *Fgf23, Adamts9,* and *Timp1* exhibited substantial expression level differences. In addition, levels of *Ccd1* on qRT-PCR were opposite of the microarray data. Cells were sorted as in Figure 3**.** Relative mRNA levels of selected genes where the average lower expressing set of samples were arbitrarily set to 1. Each bar represents the average of three independent experiments (±s.d.). *P < 0.05, **P < 0.01, ***P < 0.001.

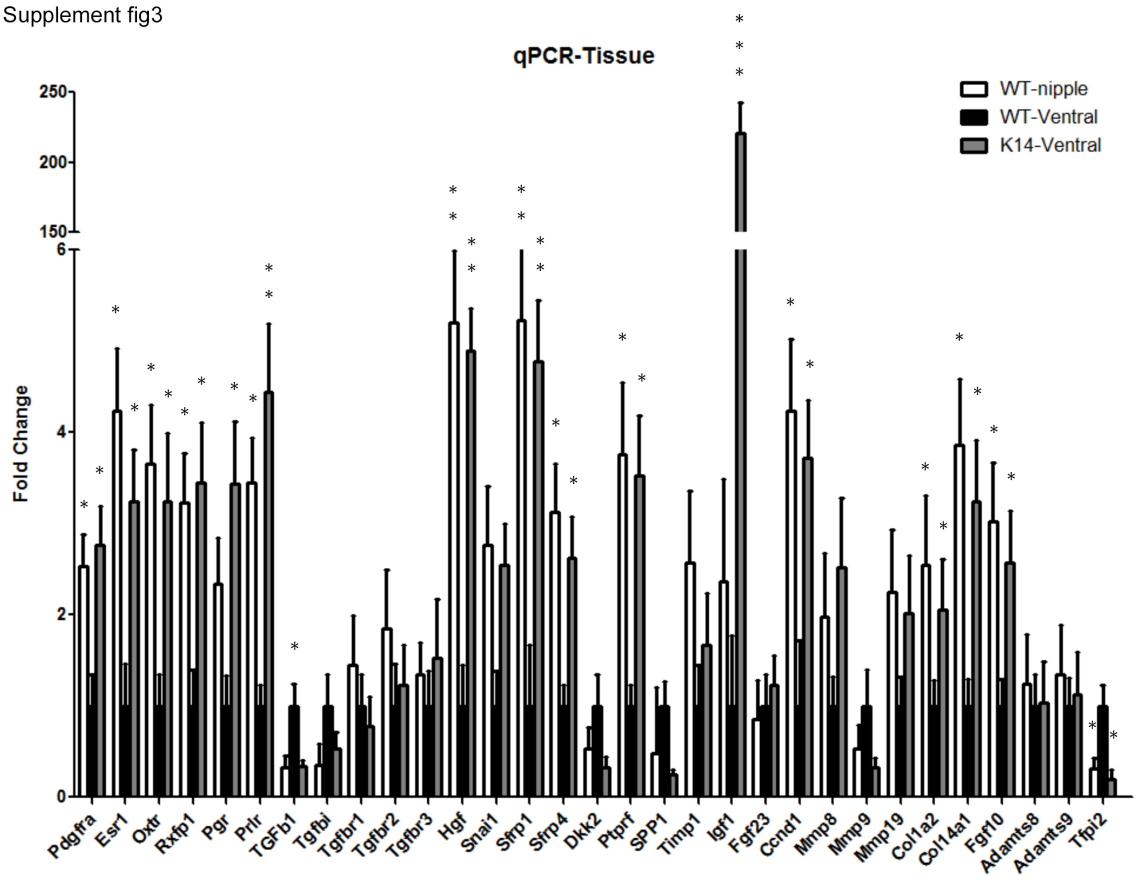

Supplemental Figure 3. Confirmation of select differentially expressed genes by qRT-PCR using RNA from intact tissues. To determine if the differential gene expression pattern of KrP fibroblasts was representative of the intact nipple, we validated it by qRT-PCR on RNA from the micro dissected nipples WT and KrP ventral skin. Indeed, all transcripts with the exception of the genes noted in figure 2 , were either elevated or reduced in the WT nipple as compared to WT non-nipple ventral skin in accordance with the KrP-to-WT fibroblasts differences (Fig. S3). In addition, *Igf1* expression was substantially lower (by ~100 fold) in the intact WT nipple as compared to KrP fibroblasts, or intact KrP ventral skin (Fig. S2, S3). Relative mRNA levels of selected genes where the WT ventral skin samples were arbitrarily set to 1. Each bar represents the average of three independent experiments (±s.d.). *P < 0.05, **P < 0.01, ***P < 0.001.

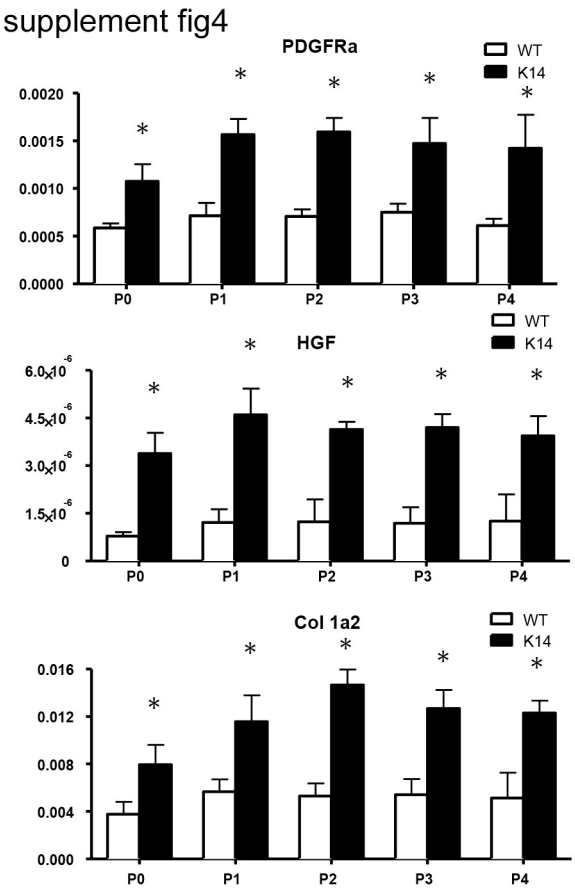

Supplemental Figure 4. Differential gene expression is maintained *in vitro*.

(A-D) To determine if the nipple fibroblast signature was stable in culture, we grew both WT and KrP ventral fibroblasts *in vitro* for up to 5 passages. We evaluated three signature transcripts (*Col1a*, *Pdgfrα* and *Hgf)* and found they remained differentially regulated in KrP relative to WT ventral fibroblasts, suggesting that some gene expression studies can be performed with cells grown *in vitro*. Relative mRNA levels in primary cultured fibroblasts at various passages. Expression of these transcripts was measured by qRT-PCR and normalized to *Gapdh* using absolute method. Each bar represents the average of three independent experiments (±s.d.). *P < 0.05.

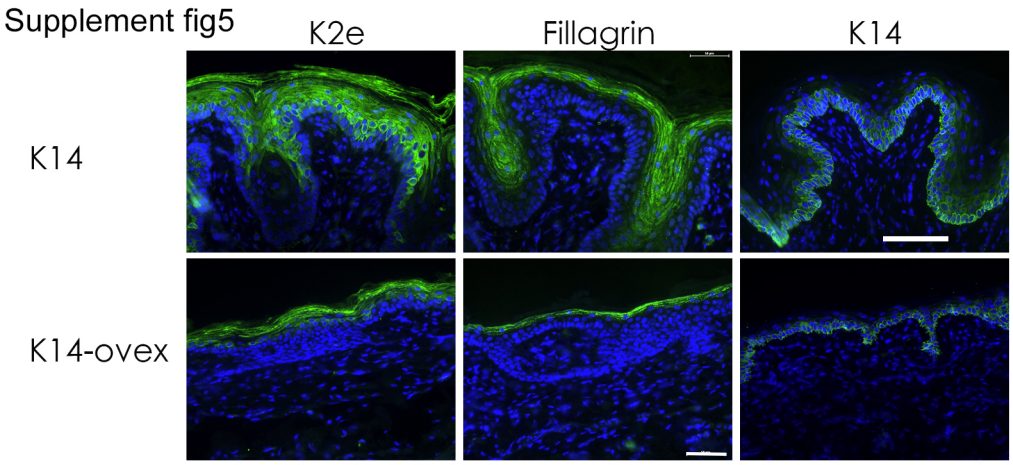

Supplemental Figure 5. Differentiation marker expression in ovexed KrP skin. Samples are indicated on the left and antibody used on the top. Layers of K2e, filaggrin and K14 antibody labeled cells are markedly diminished in ovexed mice. . Scale bar: 50uM

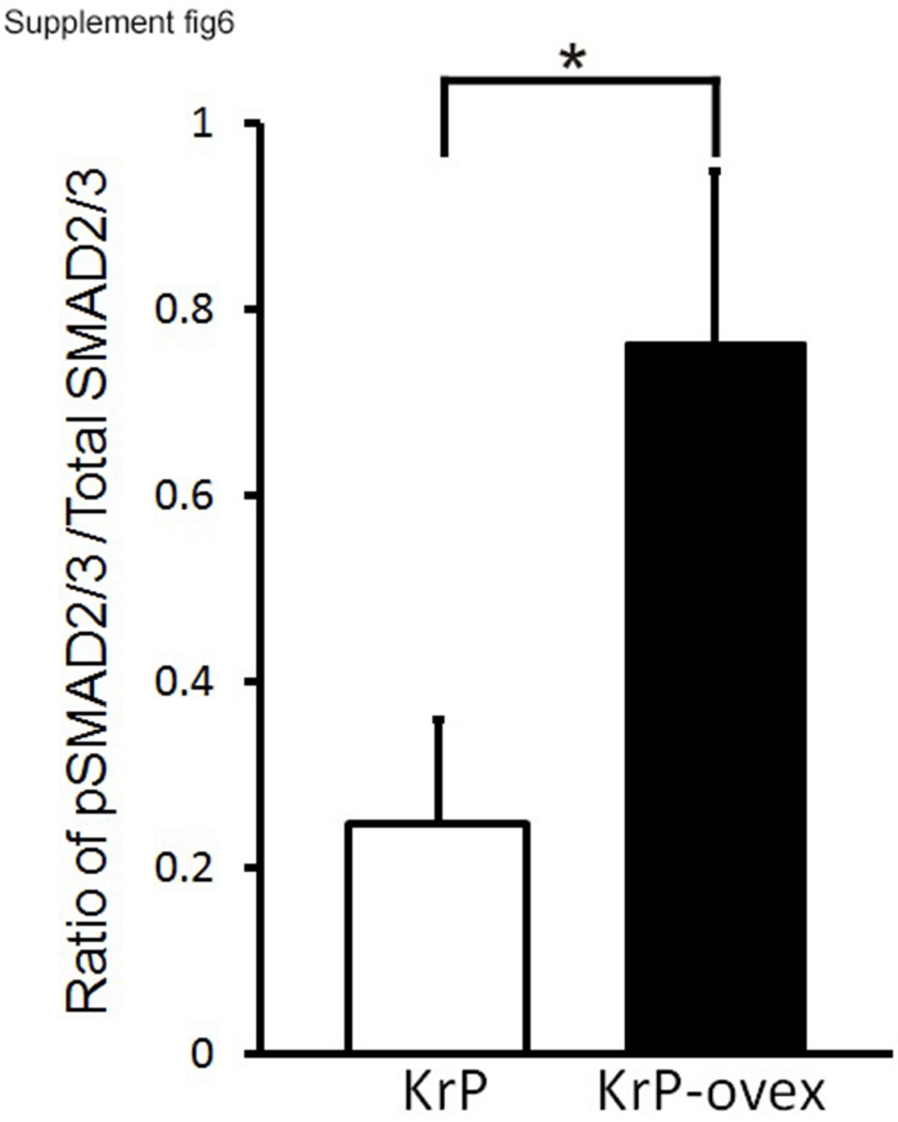

Supplemental Figure 6. Densitometry of pSmad2/3 *vs.* Smad2/3. Western blot shown in Fig. 6H was analyzed using imageJ to determine each band density. A ratio of pSmad2/3 *vs.* total Smad2/3 was calculated for KrP and ovexed KrP mice samples. Each bar represents the average ±s.d. of the triplicate samples blotted together. Extracts were evaluated two times in this manner with similar results. *P < 0.05.

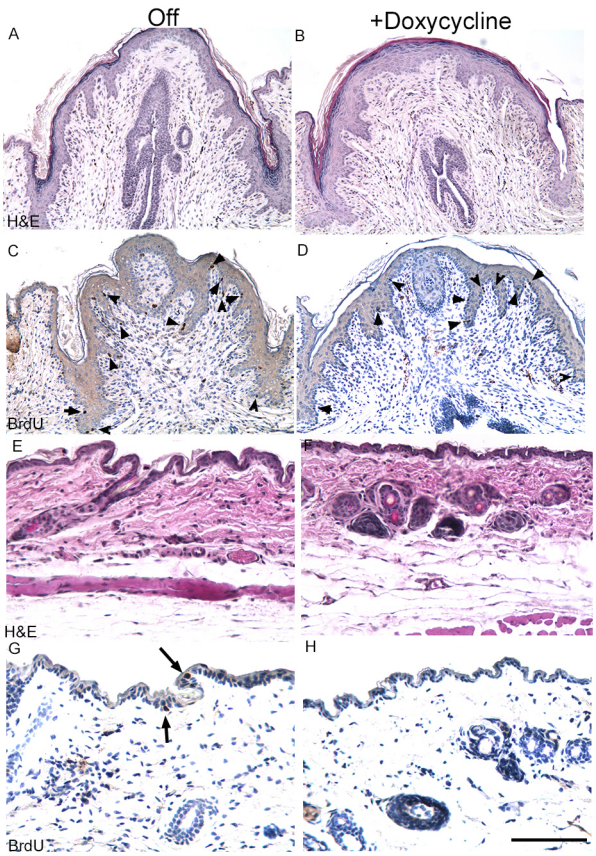

Supplement fig7

Supplemental Figure 7. Overexpression of TGFβ1 in the epidermis. Six-week-old *K14-rTA/tetO-TGF β1* virgin mice were either placed on doxycycline chow or control chow for 3-weeks, injected with BrdU and harvested. Number 4 and 5 nipples as well as non-nipple skin samples were processed for H&E and BrdU staining. **A, C, E** and **G** sections are from untreated controls and **B, D, F** and **H** from doxycycline treated animals. Nipple samples are **A-D** and ventral skin samples are **E-H.** Scale bar: 190 μm in A-D, 380 μm in E-H. Changes in the ventral epidermis of the TGFβ1 overexpressing mice were readily apparent in that portions of it pealed off during hair removal. Treatment of WT C57BL/6 mice with doxycycline chow failed to produce any detectable changes in the nipple or epidermis (not shown).

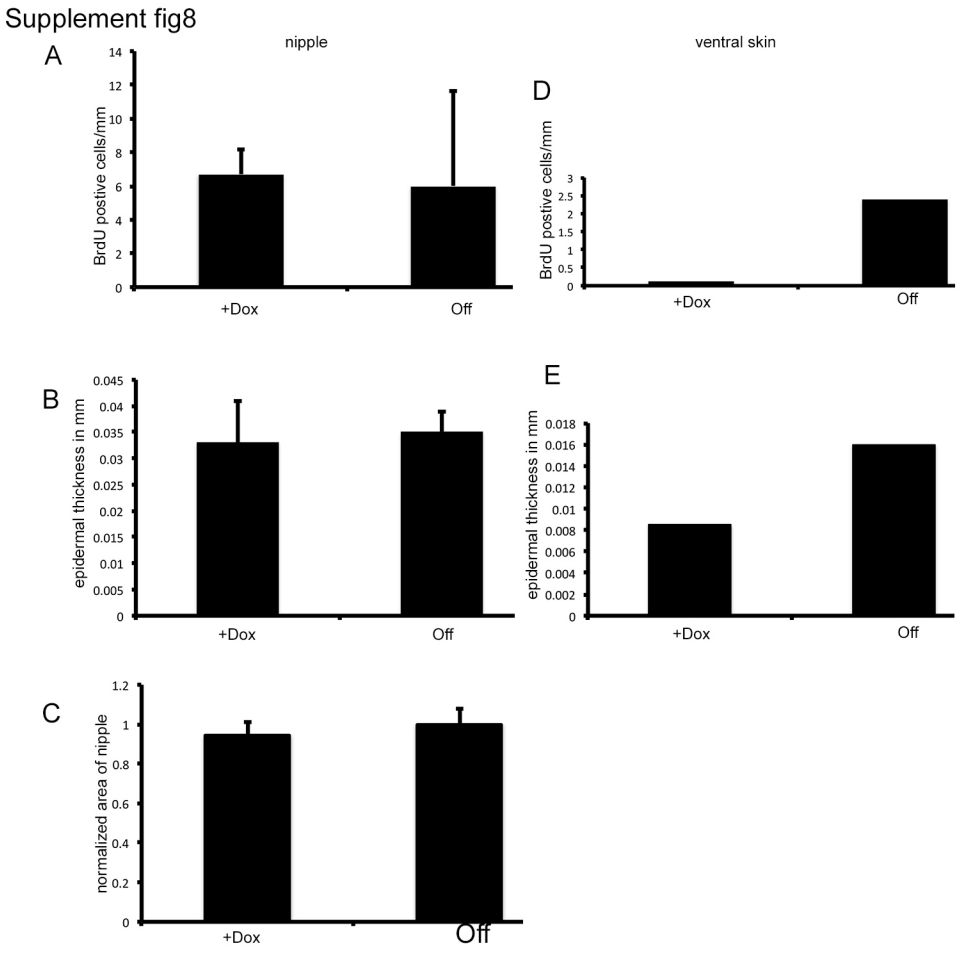

Supplemental Figure 8. BrdU analysis. Sections of eight nipples were analyzed using imageJ for **(A)** BrdU positive cells per epidermal/dermal junction length; **(B)** nipple epidermal thickness; **(C)** nipple area. No statistically significant differences in any of these parameters were observed between doxycycline treated nipples and those of controls. **(D)** BrdU positive cells per epidermal/dermal junction length and **(E)** epidermal thickness were evaluated for the ventral epidermis of the animals (n=2) and these parameters were markedly reduced in doxycycline treated animals.

Supplemental Methods

Isolation of adult fibroblasts

The collagenase solution contained 1.25 mg/ml Collagenase type I (Gibco Thermo Fisher Scientific, Waltham, MA), 0.5 mg/ml Collagenase type II (Worthington Biochemical Co., Lakewood, NJ), 0.5 mg/ml Collagenase type IV (Sigma-Aldrich, St. Louis, MO), and 50 U/ml DNase I (Worthington Biochemical Co., Lakewood, NJ) in DMEM media at 37°C for one hour. The preparations were then passed through blunt-end needles several times to mechanically dissociate dermis before filtering the mixture through a 70 μm strainer.

Note that the ventral dermis of WT mice would contain a very small number of nipple fibroblasts.

Histology and immunofluorescence

Samples were collected, fixed and sectioned as previously described (Wu et al., 2015). The following primary antibodies against the following proteins were used: vimentin (mouse monoclonal, ab28028, Abcam, Cambridge MA), smooth muscle actin 1:50 (mouse monoclonal, A2547, Sigma-Aldrich, St. Louis MO), cytokeratin 2e 1:500 (mouse monoclonal 10R-C166a, Fitzgerald, Acton, MA), Keratin 14 (rabbit polyclonal, 905301, BioLegend, San Diego, CA), filaggrin 1:5,000 (rabbit polyclonal, 905801, BioLegend, San Diego, CA), Pdgfrα 1:200 (goat polyclonal, AF1062, R&D systems, Minneapolis MN and C-9 Santa Cruz Biotechnology, Dallas, TX), Esr1 (rabbit polyclonal, HC-20, Santa Cruz Biotechnology, Dallas, TX), Smad2/3 (rabbit polyclonal, FL-425, Santa Cruz Biotechnology, Dallas, TX),

pSmad2/3 1:200 (goat polyclonal, sc-11769, Santa Cruz Biotechnology, Dallas, TX). Secondary antibodies were used at 1:200 to 1:500 dilution (Jackson Immuno Research Laboratories Inc., West Grove, PA), including Alexa-Fluor 488 or 647- conjugated goat anti-rabbit or anti-mouse IgG. Nucleus staining was conducted using DAPI (D1306, Thermo Fisher Scientific, Waltham, MA) or Draq5 (62251, Thermo Fisher Scientific, Waltham, MA).

Western Blotting

The following primary antibodies were used: ERa (rabbit polyclonal, HC-20, Santa Cruz Biotechnology, Dallas, TX), Smad2/3 (rabbit polyclonal, FL-425, Santa Cruz Biotechnology, Dallas, TX), pSmad2/3 (sc-11769R, Santa Cruz Biotechnology, Dallas, TX). For the tissue analysis the following antibodies were used: β-tubulin 1:125 (mouse monoclonal, E7-s, Developmental Studies Hybridoma Bank, Iowa City IA), p-Smad2/3 (Ser 423/425) 1:100 (rabbit polyclonal, sc-11769, Santa Cruz Biotechnology, Dallas, TX), Smad2/3 (C-8) 1:200 (mouse monoclonal, sc-133098, Santa Cruz Biotechnology, Dallas, TX).

Supplementary Tables

Supplementary table S1. Microarray gene expression data and analysis. Data are generated from sorted Pdgfrα-positive ventral KrP and WT fibroblasts. Tab 1, raw gene expression data; tab 2, list of up-regulated genes; tab 3, list of down-regulated genes; tab 4, select signaling pathway genes; tab 5, reference signaling pathway gene list.

Click here to Download Table S1

Supplementary table S2. Differential gene expression analysis on Pdgfrα-positive ventral KrP and WT fibroblasts using Network2Canvas platform. Individual tabs contains lists of enriched terms within given gene networks.

Click here to Download Table S2

Supplemental Figures

Supplementfig1

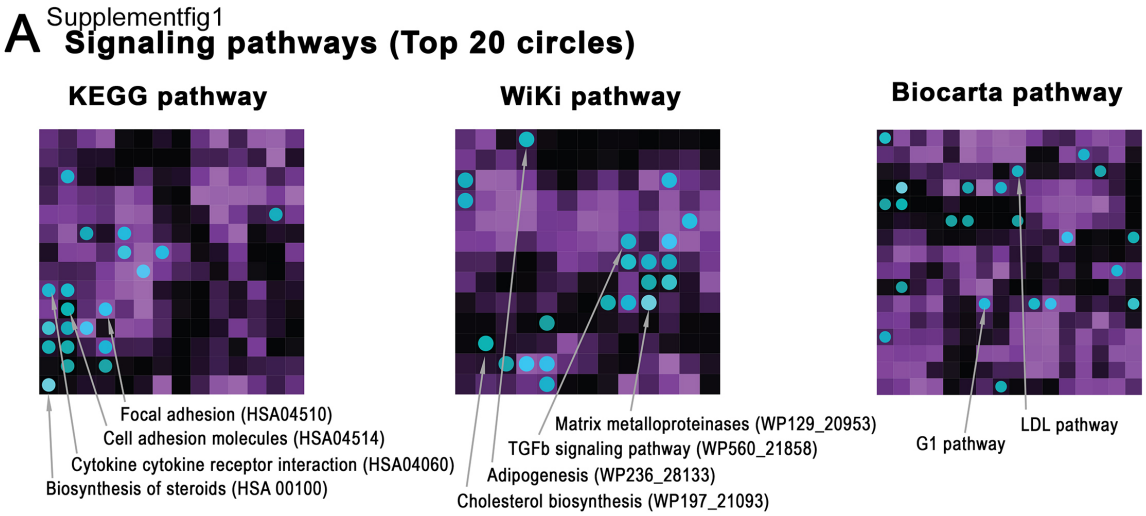

Supplemental figure S1. Network2Canvas analysis of KrP *vs.* WT ventral fibroblasts for seven gene-set libraries. Signaling pathways **(A),** Transcription **(B),** Kinase enrichment analysis **(C),** and Gene ontology and Cancer cell line encyclopedia **(D).** Each canvas represents a specific gene-set library, where each square represents a gene list linked with a gene-set library group. Square brightness is determined by its similarity to its eight neighbors. Each circle (blue) represents top 20 enriched pathways using KrP *vs.* WT DEGs within specific gene set library. Only relevant and statistically significant pathways are selectively annotated. Also see Supplementary tables S1 and S2.

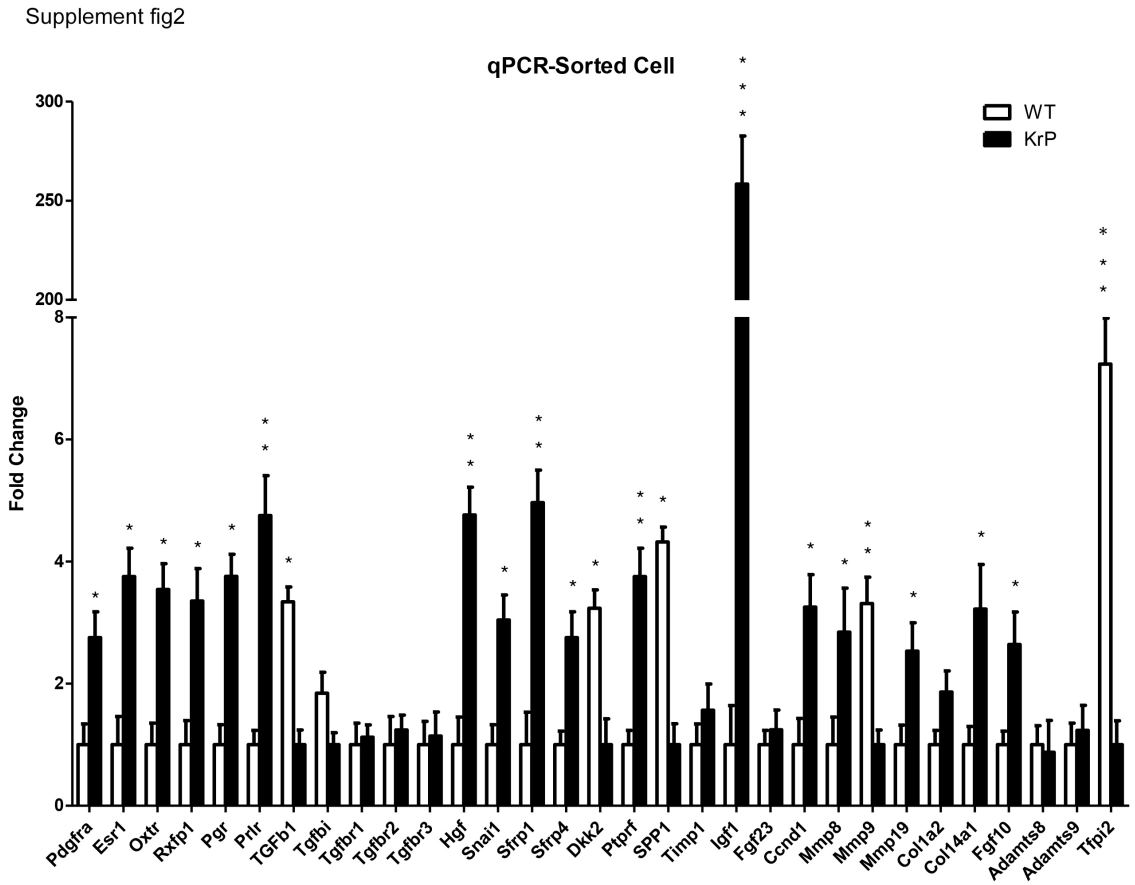

Supplemental Figure S2. Confirmation of select differentially expressed genes by qRT-PCR using RNA from sorted cells. The differential expression of 30 transcripts (20 increased, 6 decreased and 4 unchanged in KrP relative to WT fibroblasts), many of which are part of the pathways identified by the Ingenuity and GO term analysis, was confirmed by qRT-PCR (Fig. S2). Of the transcripts evaluated, all with the exception of *Fgf23, Adamts9,* and *Timp1* exhibited substantial expression level differences. In addition, levels of *Ccd1* on qRT-PCR were opposite of the microarray data. Cells were sorted as in Figure 3**.** Relative mRNA levels of selected genes where the average lower expressing set of samples were arbitrarily set to 1. Each bar represents the average of three independent experiments (±s.d.). *P < 0.05, **P < 0.01, ***P < 0.001.

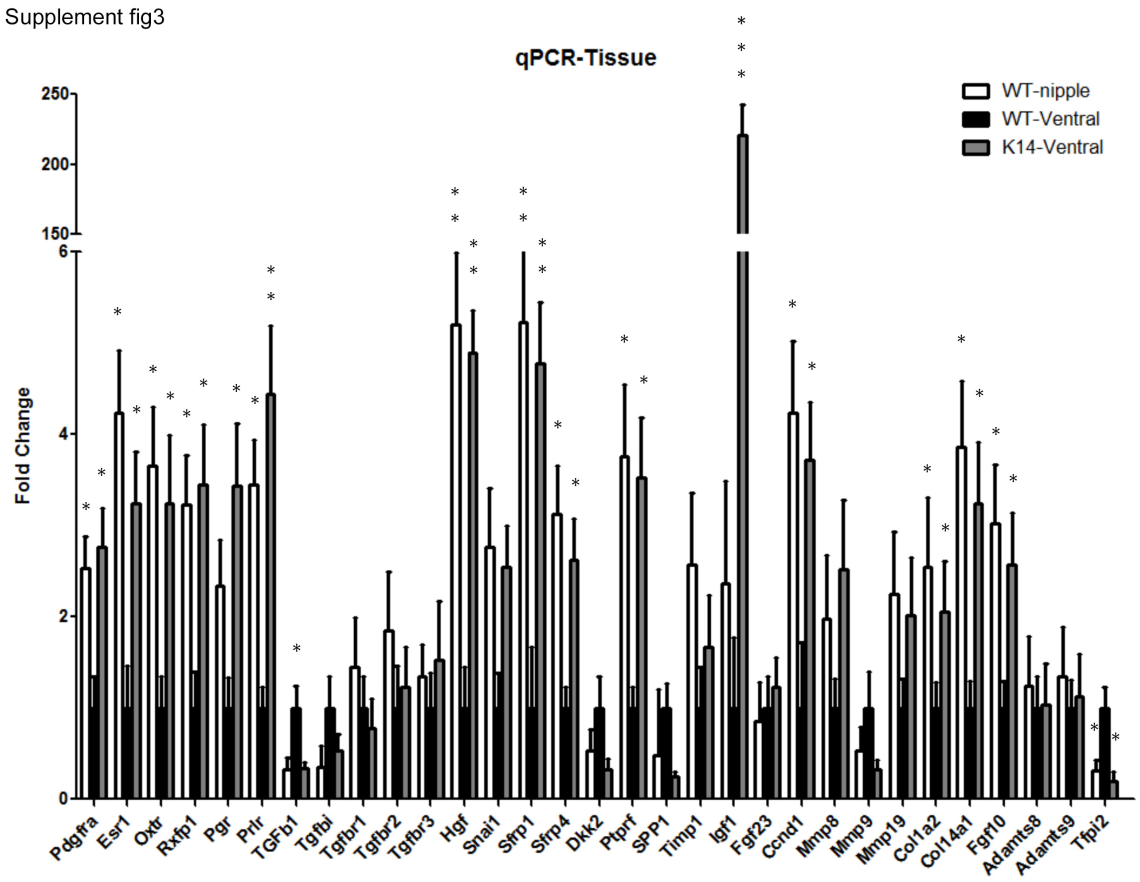

Supplemental Figure S3. Confirmation of select differentially expressed genes by qRT-PCR using RNA from intact tissues. To determine if the differential gene expression pattern of KrP fibroblasts was representative of the intact nipple, we validated it by qRT-PCR on RNA from the micro dissected nipples WT and KrP ventral skin. Indeed, all transcripts with the exception of the genes noted in figure 2 , were either elevated or reduced in the WT nipple as compared to WT non-nipple ventral skin in accordance with the KrP-to-WT fibroblasts differences (Fig. S3). In addition, *Igf1* expression was substantially lower (by ~100 fold) in the intact WT nipple as compared to KrP fibroblasts, or intact KrP ventral skin (Fig. S2, S3). Relative mRNA levels of selected genes where the WT ventral skin samples were arbitrarily set to 1. Each bar represents the average of three independent experiments (±s.d.). *P < 0.05, **P < 0.01, ***P < 0.001.

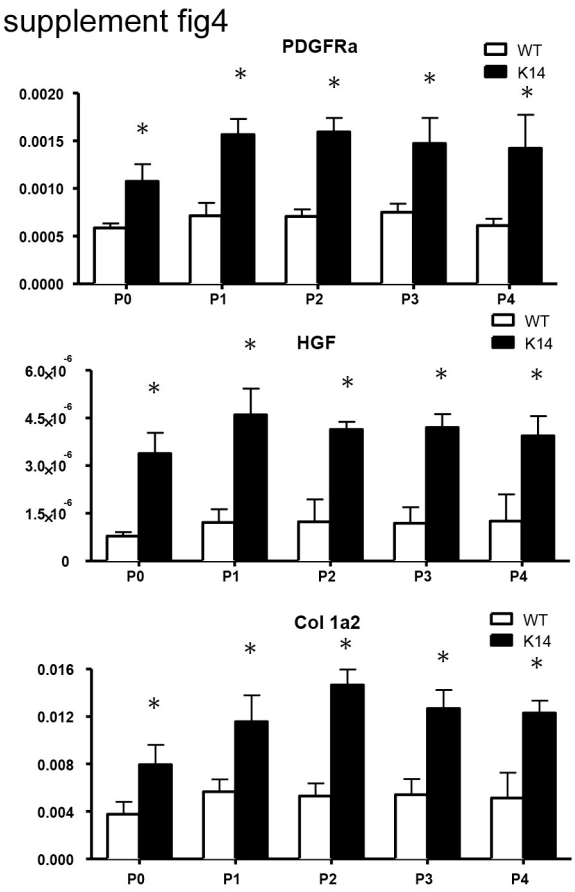

Supplemental Figure S4. Differential gene expression is maintained *in vitro*.

(A-D) To determine if the nipple fibroblast signature was stable in culture, we grew both WT and KrP ventral fibroblasts *in vitro* for up to 5 passages. We evaluated three signature transcripts (*Col1a*, *Pdgfrα* and *Hgf)* and found they remained differentially regulated in KrP relative to WT ventral fibroblasts, suggesting that some gene expression studies can be performed with cells grown *in vitro*. Relative mRNA levels in primary cultured fibroblasts at various passages. Expression of these transcripts was measured by qRT-PCR and normalized to *Gapdh* using absolute method. Each bar represents the average of three independent experiments (±s.d.). *P < 0.05.

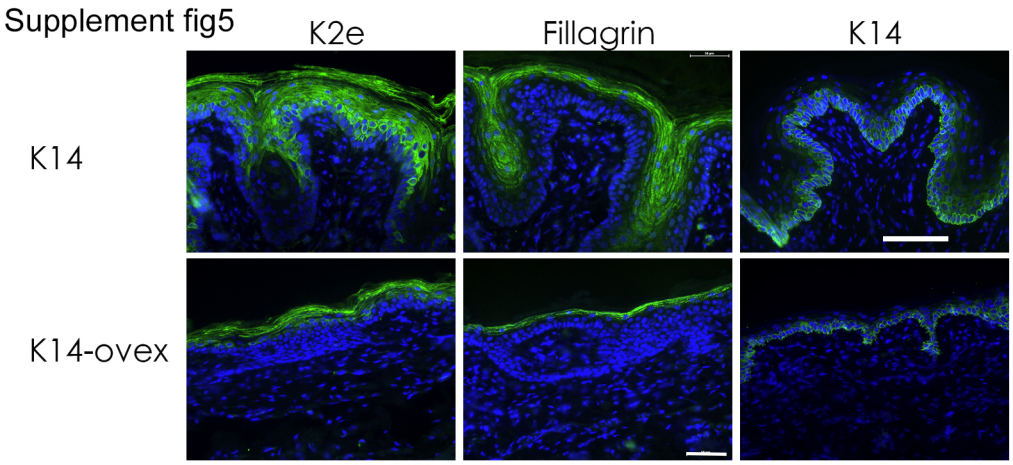

Supplemental Figure S5. Differentiation marker expression in ovexed KrP skin. Samples are indicated on the left and antibody used on the top. Layers of K2e, filaggrin and K14 antibody labeled cells are markedly diminished in ovexed mice. . Scale bar: 50μm

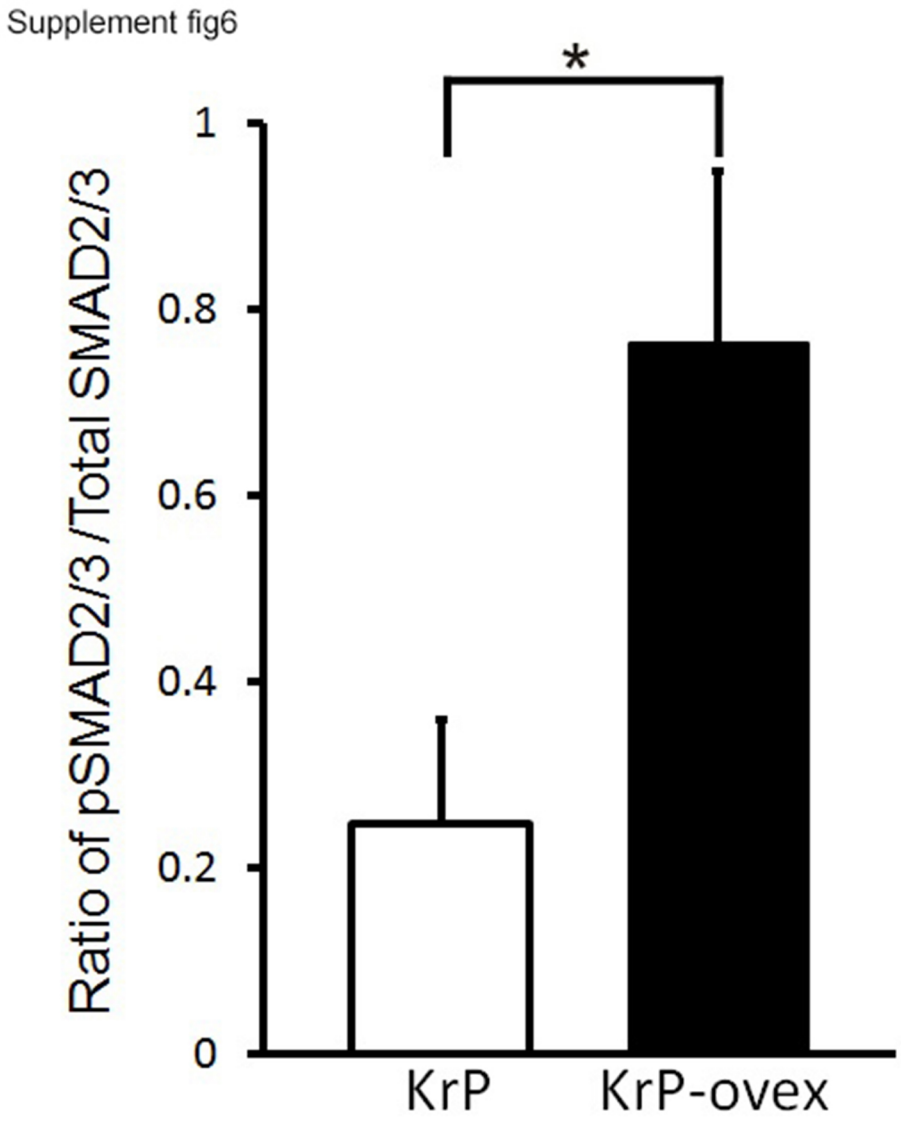

Supplemental Figure S6. Densitometry of pSmad2/3 *vs.* Smad2/3. Western blot shown in Fig. 6H was analyzed using imageJ to determine each band density. A ratio of pSmad2/3 *vs.* total Smad2/3 was calculated for KrP and ovexed KrP mice samples. Each bar represents the average ±s.d. of the triplicate samples blotted together. Extracts were evaluated two times in this manner with similar results. *P < 0.05.

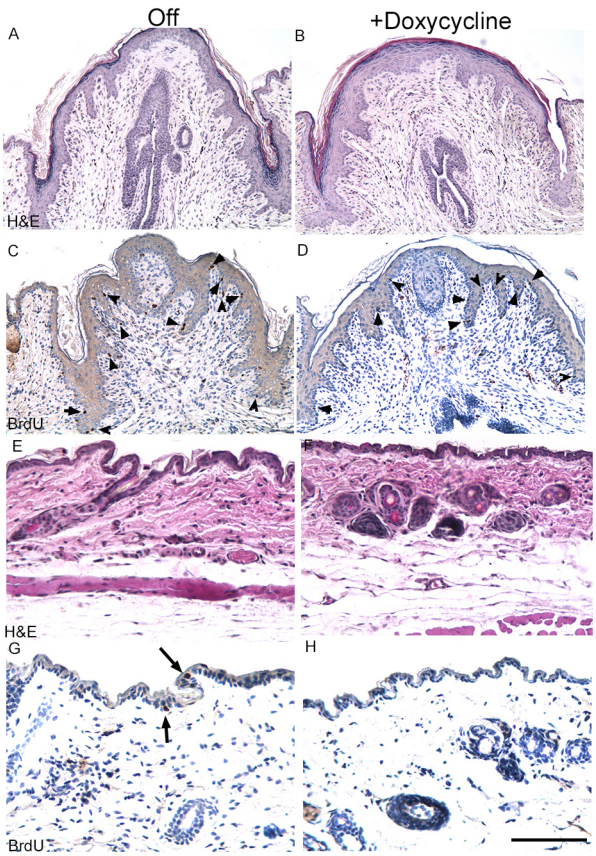

Supplement fig7

Supplemental Figure S7. Overexpression of TGFβ1 in the epidermis. Six-week-old *K14-rTA/tetO-TGF β 1* virgin mice were either placed on doxycycline chow or control chow for 3-weeks, injected with BrdU and harvested. Number 4 and 5 nipples as well as non-nipple skin samples were processed for H&E and BrdU staining. **A, C, E** and **G** sections are from untreated controls and **B, D, F** and **H** from doxycycline treated animals. Nipple samples are **A-D** and ventral skin samples are **E-H.** Scale bar: 190 μm in A-D, 380 μm in E-H. Changes in the ventral epidermis of the TGFβ1 overexpressing mice were readily apparent in that portions of it pealed off during hair removal. Treatment of WT C57BL/6 mice with doxycycline chow failed to produce any detectable changes in the nipple or epidermis (not shown).

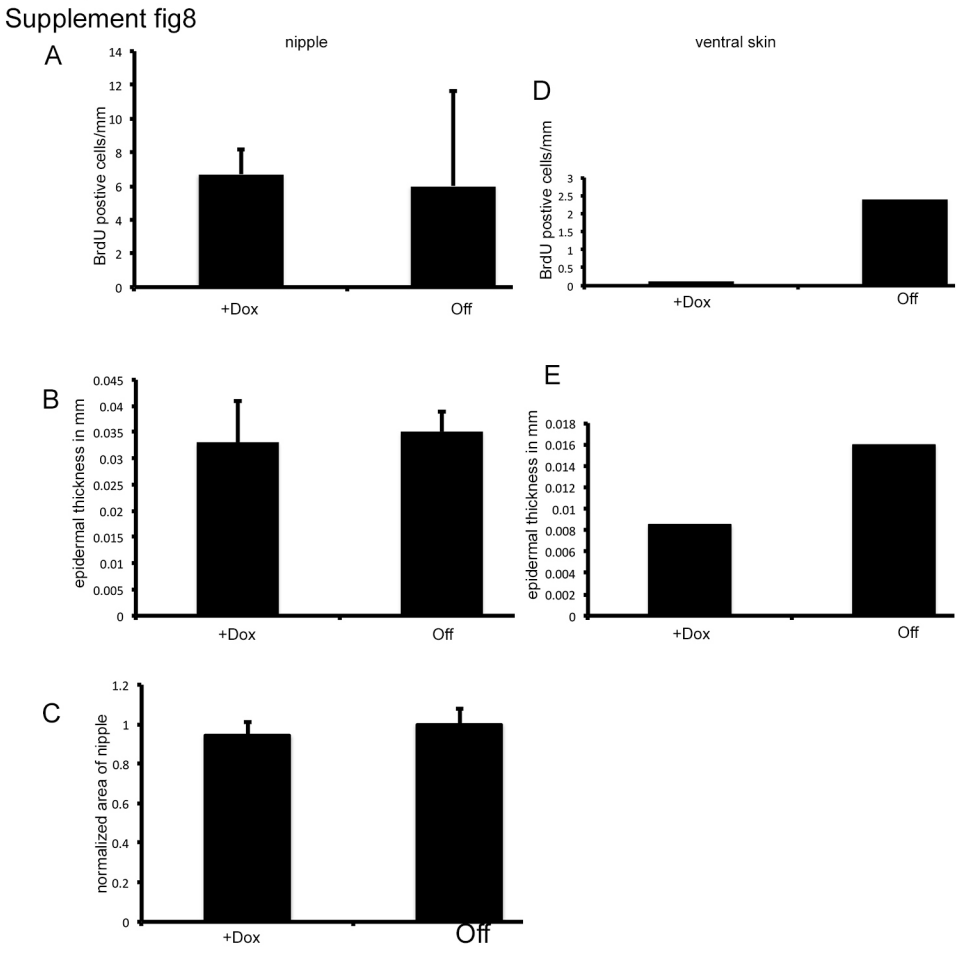

Supplemental Figure S8. BrdU analysis. Sections of eight nipples were analyzed using imageJ for **(A)** BrdU positive cells per epidermal/dermal junction length; **(B)** nipple epidermal thickness; **(C)** nipple area. No statistically significant differences in any of these parameters were observed between doxycycline treated nipples and those of controls. **(D)** BrdU positive cells per epidermal/dermal junction length and **(E)** epidermal thickness were evaluated for the ventral epidermis of the animals (n=2) and these parameters were markedly reduced in doxycycline treated animals.